ESPOO 2006 VTT PUBLICATIONS 596

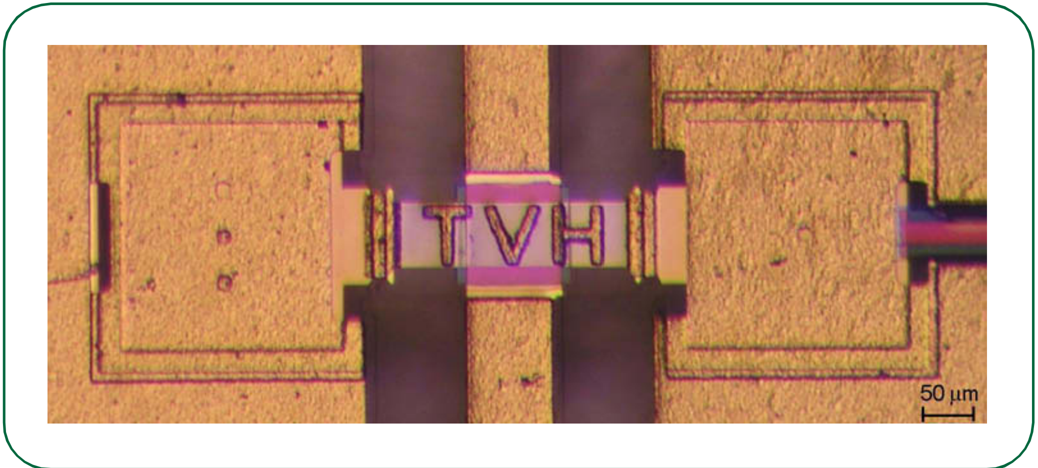

Tauno Vähä-Heikkilä

MEMS tuning and matching circuits, and millimeter wave on-wafer measurements

VTT

VTT PUBLICATIONS 596

MEMS tuning and matching circuits, and millimeter wave on-wafer measurements

Tauno Vähä-Heikkilä

Dissertation for the degree of Doctor of Science in Technology to be presented with due permission of the Department of Electrical and Communications Engineering for public examination and debate in Auditorium S4 at the Helsinki University of Technology (Espoo, Finland) on the 27th of March, 2006, at 12 o'clock noon.

ISBN 951–38–6704–8 (soft back ed.)
ISSN 1235–0621 (soft back ed.)

ISBN 951–38–6705–6 (URL: http://www.vtt.fi/inf/pdf/)
ISSN 1455–0849 (URL: http://www.vtt.fi/inf/pdf/)

Copyright © VTT Technical Research Centre of Finland 2006

JULKAISIJA – UTGIVARE – PUBLISHER

VTT, Vuorimiehentie 3, PL 1000, 02044 VTT
puh. vaihde 020 722 111, faksi 020 722 4374

VTT, Bergsmansvägen 3, PB 1000, 02044 VTT
tel. växel 020 722 111, fax 020 722 4374

VTT Technical Research Centre of Finland, Vuorimiehentie 3, P.O. Box 1000, FI-02044 VTT, Finland
phone internat. +358 20 722 111, fax +358 20 722 4374

VTT, Tietotie 3, PL 1000, 02044 VTT
puh. vaihde 020 722 111, faksi 020 722 7012

VTT, Tietotie 3, PB 1000, 02044 VTT
tel. växel 020 722 111, fax 020 722 7012

VTT Technical Research Centre of Finland, Tietotie 3, P.O. Box 1000, FI-02044 VTT, Finland
phone internat. +358 20 722 111, fax +358 20 722 7012

Otamedia Oy, Espoo 2006

Vähä-Heikkilä, Tauno. MEMS tuning and matching circuits, and millimeter wave on-wafer measurements [Mikromekaaniset viritys- ja sovituspiirit sekä millimetriaaltoalueen suoraan kiekolta tehtävät mittaukset]. Espoo 2006. VTT Publications 596. 86 p. + app. 82 p.

Keywords RF MEMS, on-wafer measuring techniques, millimeter wave devices, impedance tuning, instrumentation, noise parameter measurements, reconfigurable matching networks, W-band measurement, double-stub tuners, triple-stub tuners, amplifier applications

Abstract

The focus of this thesis is on the development of on-wafer measurement techniques for millimeter wave device and circuit characterization as well as on the development of MEMS based impedance tuning circuits both for measurement and telecommunication applications. Work done in this thesis is presented with eight scientific articles written by the author. The summary of the thesis introduces the field of on-wafer measurements and impedance tuning methods, and is followed by the articles.

Wide-band on-wafer measurement systems have been developed for noise parameter measurement at room temperature at W-band, and for cryogenic S-parameter measurements at 50–110 GHz and 20–295 K. Using the developed systems, noise parameters of an InP HEMT have been measured and results are shown in the frequency band of 79–94 GHz. These are the first published noise parameter measurement results for an active device at W-band, and first on-wafer measurement results at cryogenic conditions and at 50–110 GHz.

Novel RF MEMS impedance tuners have been developed for instrumentation and measurement applications to improve measurement automation and accuracy in on-wafer measurements. Several integrated impedance tuners have been realized to cover 6–120 GHz frequency range. RF MEMS technology has also been used for reconfigurable matching networks. Reconfigurable distributed 4–18 GHz and 30–50 GHz matching networks have been designed, fabricated, and characterized. These are based on switched 4 or 8 MEMS capacitors producing 16 or 256 different impedances. The matching networks are ideal for multi-band and wide impedance range amplifier as well as for antenna matching and tuning applications. Both the tuners and matching networks have shown state-of-the-art performance for circuits realized with integrated circuit technologies.

Vähä-Heikkilä, Tauno. MEMS tuning and matching circuits, and millimeter wave on-wafer measurements [Mikromekaaniset viritys- ja sovituspiirit sekä millimetriaaltoalueen suoraan kiekolta tehtävät mittaukset]. Espoo 2006. VTT Publications 596. 86 s. + liitt. 82 s.

Avainsanat RF MEMS, on-wafer measuring techniques, millimeter wave devices, impedance tuning, instrumentation, noise parameter measurements, reconfigurable matching networks, W-band measurement, double-stub tuners, triple-stub tuners, amplifier applications

Tiivistelmä

Väitöskirjatyössä kehitettiin suoraan kiekolta tehtäviä millimetriaaltoalueen mittauksia sekä mikromekaanisia (MEMS) impedanssin säätö- ja sovituspiirejä.

Mittauslaitteistoja ja -menetelmiä kehitettiin suoraan kiekolta tehtäviin mittauksiin millimetriaaltoalueelle. Kohinaparametrien mittaamiseksi kehitettiin laitteisto W-alueelle (75–110 GHz), ja mittaustulokset esitetään InP HEMT -transistorille 79–94 GHz taajuusalueella. Sirontaparametrien mittaamiseksi kryogeenisissä olosuhteissa kehitettiin laitteisto W-alueelle, ja laajakaistaiset sekä kahden aaltoputkikaistan kattavat mittaustulokset esitetään InP HEMT -transistoreille 50–110 GHz:n taajuusalueella ja 20–295 K:n lämpötiloissa. Sekä molemmat mittauslaitteistot että esitettävät tulokset ovat ainutlaatuisia näillä taajuuksilla.

Kohinaparametrimittauslaitteistojen kehittämiseksi ja mittausten automatisoimiseksi väitöskirjatyössä suunniteltiin ja valmistettiin integroituja mikromekaanisia impedanssivirittimiä. Impedanssivirittimillä tuotetaan erilaisia impedansseja, ja niitä voidaan kontrolloida sähköisesti. Impedanssin säätö perustuu MEMS-kondensaattoreihin, ja kehitetyillä piireillä saadaan tuotettua tuhansia erilaisia impedansseja riippuen MEMS-kondensaattoreiden lukumäärästä. Impedanssivirittimiä kehitettiin usealle eri taajuusalueelle taajuuksien 6 ja 120 GHz välille. Virittimien tuottama heijastuskerroin on parhaimmillaan lähellä yhtä mitatun seisovan aallon suhteen ollessa 199 taajuudella 30 GHz. Työssä myös sovellettiin MEMS-kondensaattoreita impedanssinsovituspiireihin tehovahvistimen ja antennin sovittamiseksi. Piireissä integroidun siirtolinjan sähköistä pituutta ja impedanssia muutetaan. Mitatut tulokset osoittavat, että piireillä voidaan sovittaa paljon erilaisia impedansseja pienin häviöin ja lineaarisesti.

Preface

I would like to thank everyone who allowed me to meet this important goal in my life. I wish to thank my advisor Research Professor Jussi Tuovinen at VTT for all his support, leadership, and encouragement during the thesis work.

Professor Antti Räisänen at the Helsinki Univ. of Technology contributed to this thesis in the finalization of the thesis and in the review process. His valuable comments are greatly appreciated.

I'm very thankful for Proferssor Gabriel M. Rebeiz for taking me to his group, sharing all his knowledge, guiding me during my stay at the Univ. of Michigan and also after that, and his friendship.

I am grateful to Dr. Jeremy Muldavin and Dr. Michael Schlechtweg for their valuable comments and pre-examination of the thesis. I'm also thankful to the opponent Prof. Herbert Zirath for agreeing to examine the thesis.

I would like to thank all people in MilliLab and the former Radio Technology Group at VTT: Alpo Ahonen, Hannu Hakojärjvi, Markku Jenu, Mikko Kantanen, Timo Karttaavi, Anna Karvonen, Dr. Arttu Luukanen, Ilkka Marttila, Pekka Rantakari, Markus Rintamäki, Hannu Salminen, Dr. Jussi Varis, and Juha Volotinen, as well as people in other teams at VTT: Ari Alastalo, Prof. Hannu Kattelus, Anu Kärkkäinen, Markku Sipilä, Jussi Säily, and Mari Ylönen. I'm very thankful for Research Professor Aarne Oja for his guidance and support during my stay at VTT. I would like to thank Aija Kaski and Milja Heimonen for arranging my numerous travels all around the world.

I am grateful to all people of TICS group that I had possibility to get to know you in Michigan. First of all, Dr. Jad Rizk, who was my mentor in the clean room and Lebanese culture, and with whom I experienced many things both inside and outside of the clean room. Also, I have enjoyed the friendship of other lab-mates, Dr. Laurent Dussopt, Dr. Jose Canillas, Dr. Abbas Abbaspoor-Tamijani, Dr. Bernhard Schoenlinner, Dr. Kamran Entesari, Dr. Bryan Hung, Dr. Timothy Hancock, Dr. Andrew Brown, Dr. Kiran Nimmagada, Noriyo Nishijima, Koen van Caekenberghe, Michael Chang, Carson White, Chris Galbraight, San-June Park, Byung-Wook Min, Philip Grajek, and Helena Chan.

I would like to thank all of my Lebanese friends who were my family during my stay in the US. In addition to Gabriel and Jad, I'm thankful for Elias Abboud, Pierre Assouad, Walid El Asmar, Fadi Zoghby, Prof. Imad Btaich, and Tony Nawar.

I wish to thank Dr. Tapani Närhi from ESA, ESTEC, for his valuable comments in European Space Agency (ESA) funded projects as well as his encouragement during this thesis work.

This work has been carried out in 2000–2005 at MilliLab, VTT Technical Research Centre of Finland and the University of Michigan in projects funded by VTT, ESA, and DARPA IRFEE program. I would also like thank Graduate School of Electronics, Telecommunications, and Automation (GETA), Nokia Foundation, and Foundation of the Finnish Society of Electronics Engineers.

I would like to thank my parents Mirja-Leena and Jorma as well my sister Kaisa and brothers Kalle and Frans for their support. Finally, I would like to thank my wife Sini for her support and patience during the years.

Tauno Vähä-Heikkilä, Espoo, March 2005.

List of publications

[P1] T. Vähä-Heikkilä, M. Lahdes, M. Kantanen, and J. Tuovinen, "On-wafer noise parameter measurements at W-band." *IEEE Transactions on Microwave Theory and Techniques*, Vol. 51, no. 6, pp. 1621–1628, 2003.

[P2] T. Vähä-Heikkilä, J. Varis, H. Hakojärvi, and J. Tuovinen, "Cryogenic on-wafer measurements at 50–110 GHz and at 20–295 K." *Proceedings of the 33rd European Microwave Conference*, Munich, Germany, 2003. Pp. 1167–1170.

[P3] T. Vähä-Heikkilä, K. Van Caekenberghe, J. Varis, J. Tuovinen, and G.M. Rebeiz, "RF MEMS impedance tuners for 6–24 GHz applications." *Accepted for publication in International Journal of RF and Microwave Computer-Aided Engineering,* February 2006.

[P4] T. Vähä-Heikkilä, J. Varis, J. Tuovinen, and G.M. Rebeiz, "A 20–50 GHz RF MEMS single-stub impedance tuner." *IEEE Microwave and Wireless Components Letters*, vol. 15, no. 4, pp. 205–207, 2005.

[P5] T. Vähä-Heikkilä, J. Varis, J. Tuovinen, and G.M. Rebeiz, "A V-band single-stub RF MEMS impedance tuner." *Proceedings of the 34th European Microwave Conference,* Amsterdam, Netherlands, 2004. Pp. 1301–1304.

[P6] T. Vähä-Heikkilä, J. Varis, J. Tuovinen, and G.M.Rebeiz, "W-band RF MEMS double and triple-stub impedance tuners." *2005 IEEE MTT-S International Microwave Symposium Digest,* Long Beach, CA, USA, 2005. Pp. 923–926.

[P7] T. Vähä-Heikkilä, and G.M. Rebeiz, "A 4–18 GHz reconfigurable RF MEMS matching network for power amplifier applications." *International Journal of RF and Microwave Computer-Aided Engineering*, Vol. 14, no. 4, pp. 356–372, 2004.

[P8] T. Vähä-Heikkilä, and G.M. Rebeiz, "A 20–50 GHz reconfigurable matching network for power amplifier applications." *2004 IEEE MTT-S International Microwave Symposium Digest,* Forth Worth, TX, USA, 2004. Pp. 717–721.

Contribution of the author in [P1–P8] is described on the next page. Furthermore, work relevant to the thesis including contribution of the author is also presented in [1–6].

Contribution of author

Contribution of the author of this thesis is the following in publications P1–P8:

[P1] The author developed the set-up and computational methods used in noise parameter measurements, under the supervision of M. Lahdes, M. Kantanen, and Prof. J. Tuovinen.

[P2] The author developed the system together with the co-authors. The author carried out measurements and data analysis. Dr. J. Varis and Prof. J. Tuovinen supervised the work.

[P3] The author designed, fabricated, and measured circuits under the supervision of Prof. G. M. Rebeiz. Dr. J. Varis and Prof. J. Tuovinen collaborated in the preliminary selection of tuner topologies and definitions of specifications. K. Van Caekenberghe built a bias control board.

[P4] The author designed, fabricated, and measured circuits under the supervision of Prof. G. M. Rebeiz. Dr. J. Varis and Prof. J. Tuovinen collaborated in the preliminary selection of tuner topologies and definitions of specifications.

[P5] The author designed, fabricated, and measured circuits under the supervision of Prof. G. M. Rebeiz. Dr. J. Varis and Prof. J. Tuovinen collaborated in the preliminary selection of tuner topologies and definitions of specifications.

[P6] The author designed, fabricated, and measured circuits under the supervision of Prof. G. M. Rebeiz. Dr. J. Varis and Prof. J. Tuovinen collaborated in the preliminary selection of tuner topologies and definitions of specifications.

[P7] The author designed, fabricated, and measured circuits. Prof. G. M. Rebeiz supervised the work.

[P8] The author designed, fabricated, and measured circuits. Prof. G. M. Rebeiz supervised the work.

Contents

Abstract 3

Tiivistelmä 4

Preface 5

List of publications 7

Contribution of author 9

Abbreviations 12

List of symbols 15

1. Introduction 17
   - 1.1 Short introduction to millimeter wave low noise receivers 18
   - 1.2 Research problem of this thesis 20
   - 1.3 Scope and contents of this thesis 21
   - 1.4 New scientific results 22

2. Millimeter wave on-wafer measurement techniques 23
   - 2.1 Cryogenic on-wafer measurements at V- and W-band 23
   - 2.2 On-wafer noise parameter measurements 26

3. Reconfigurable RF MEMS impedance tuners and matching networks 34
   - 3.1 Tuner topologies 39
     - 3.1.1 Stub-based impedance tuners 39
     - 3.1.2 Slug tuners 43
   - 3.2 Components for electrically controllable impedance tuners 44
     - 3.2.1 Varactor diodes and transistors 44
     - 3.2.2 MEMS switches and varactors 45
     - 3.2.3 Sliding planar backshorts 54
   - 3.3 Realized impedance tuners 55
     - 3.3.1 Active device based impedance tuners and matching networks 55
     - 3.3.2 Impedance tuners based on sliding planar backshorts 55
     - 3.3.3 Stub-based impedance tuners and matching networks realized with MEMS switches 55

3.3.4 Distributed impedance tuners and matching networks realized with MEMS switches 63

4. Summary of publications 67

5. Conclusion 70

References 72

Appendices

Appendix A: Detailed surface MEMS fabrication procedure used in this thesis
Publications P1–P8

Abbreviations

ALMA	Atacama Large Millimeter Array
Au	Gold
CPS	CoPlanar Stripline
CPW	CoPlanar Waveguide
DC	Direct Current
DMTL	Distributed MEMS Transmision Line
DUT	Device Under Test
ESA	European Space Agency
ESTEC	European Space Research and Technology Centre
GPIB	General-Purpose Interface Bus
HEMT	High Electron Mobility Transistor
HTS	High Temperature Superconductor
LNA	Low Noise Amplifier
LO	Local Oscillator
LRRM	Line-Reflect-Reflect-Match
MAM	Metal-Air-Metal
MAP	Microwave Anisotropy Probe
MEMS	MicroElectroMechanical Systems

MilliLab	Millimeter Wave Laboratory of Finland – MilliLab
MIM	Metal-Insulator-Metal
MMIC	Monolithic Microwave Integrated Circuit
PC	Personal Computer
PECVD	Plasma Enhanced Chemical Vapor Deposition
PMMA	Polymethylmethacrylate
RF	Radio Frequency
RIE	Reactive Ion Etching
SDA	Scracth Drive Actuator
SiCr	Silicon Chrome
Si_xN_y	Silicon Nitride
SOLT	Short-Open-Load-Thru
S-parameter	Scattering parameter
SPB	Sliding Planar Backshort
Ti	Titanium
TRL	Thru-Reflect-Line
V-Band	50–75 GHz waveguide frequency band
VLBA	Very Long Baseline Array
VNA	Vector Network Analyzer
VSWR	Voltage Standing Wave Ratio

VTT	Valtion Teknillinen Tutkimuskeskus, Technical Research Centre of Finland
W-Band	75–110 GHz waveguide frequency band
WLAN	Wireless Local Area Network
WR-10	75–110 GHz waveguide
WR-15	50–75 GHz waveguide

List of symbols

A	Area of electrodes in a capacitor
C	Capacitance of a capacitor
$C1$	Fixed capacitance
$C2$	Fixed capacitance
$C3$	Fixed capacitance
C_{FIXED}	Capacitance of a fixed capacitor
C_{MAM}	Capacitance of a metal-air-metal capacitor
C_{MEMS}	Capacitance of a MEMS switch or varactor
C_{TOT}	Total capacitance
F	Noise figure
F_{min}	Minimum noise figure
l	Transmission line length
$L_1 \ldots L_5$	Electrical length of a transmission line
L_{MEMS}	Inductance of a MEMS switch or varactor
N	Number of elements
R_{FIXED}	Resistance of a fixed capacitor
R_{MEMS}	Resistance of a MEMS switch or varactor
r_{n}	Normalized noise resistance

S1–S11	Switch numbers
Z_0	Characteristic impedance of a transmission line
$Z_1 ... Z_3$	Impedance of a transmission line
β	Propagation constant
δ	Distance between electrodes in a capacitor, gap
ε_0	Permittivity of vacuum
ε_r	Relative dielectric constant
Γ_i	Source reflection coefficient
Γ_{MAX}	Maximum reflection coefficient
Γ_{opt}	Optimum reflection coefficient

1. Introduction

Millimeter wave (30–300 GHz) technology has been traditionally used mostly in scientific and military applications, but during the last decade this technology has been applied also to commercial applications. Examples of several planned or realized radio astronomical and cosmological missions are WMAP [7], Planck [8], VLBA [9], and ALMA [10]. Commercial applications at millimeter wave lengths are, for example, automotive radars around 77 GHz e.g. [11, 12], mobile broadband telecommunication systems operating in the 62–63 GHz and 65–66 GHz bands, wireless local area networks (WLAN) in the 59–62 GHz band in Europe, and radio links at 38, 42, 58 and 94 GHz e.g. [13–16]. Millimeter wave imaging systems have also been developed both for commercial and defense applications, and they operate around 94 GHz e.g. [17–19].

High performance receivers are needed in all above mentioned applications at millimeter wave lengths. Low noise amplifiers (LNA) are key elements in these receivers and their performances have to be optimized, at least, in terms of noise, gain, and power consumption. LNAs are based on transistors, which need to be characterized and modeled before low noise amplifiers can be designed. With on-wafer measurements, devices and circuits are characterized directly from a chip or wafer. On-wafer measurements play an important role at millimeter wave frequencies and in cryogenic conditions.

As a part of integrated circuit technologies, micromachining and micro-electromechanical systems (MEMS) technologies have made their breakthrough also to millimeter wavelengths. MEMS are micro scale mechanically movable elements that are controlled electrically. The MEMS technology is applied at millimeter wavelengths, for example, for switching [20–24], phase shifting [21, 22, 24–30], filtering [31–34], impedance tuning [35, P4, P5], tunable antennas [36], and multiline-TRL calibration standards [37].

1.1 Short introduction to millimeter wave low noise receivers

Receivers have an important role in all millimeter wave scientific, defense, and commercial applications [38–41]. A simple millimeter wave receiver contains at least an antenna and a detector (Figure 1a). This kind of receiver is called a direct detection receiver. The diode detector after the antenna directly converts the millimeter wave power to voltage. In addition to the frequency selectivity of the antenna or a possible filter between the antenna and detector, the direct detection receiver does not have frequency selectivity. It is mostly suitable for applications, where the total power information of a certain frequency band is needed like in millimeter wave imaging applications or as a wideband receiver together with a narrowband swept source e.g. [17–19, 38, 39, 41]. The sensitivity of the receiver can be improved by using a low noise amplifier before the diode detector (Figure 1b). Up to-date, LNAs have been developed up to G-band (140–220 GHz) frequencies [49–51].

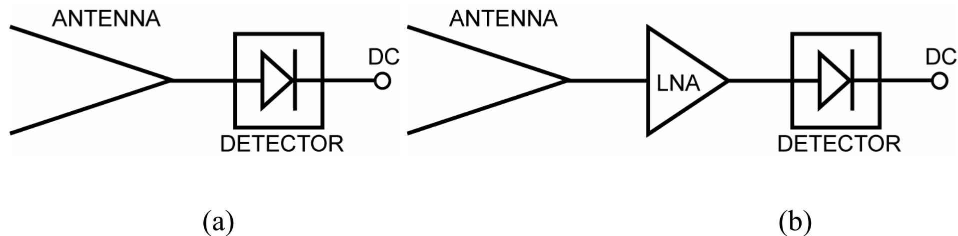

(a) (b)

Figure 1a. Schematics of a direct detection receiver, b) a direct detection receiver with an LNA.

Another common type of a receiver, used in millimeter wave applications, is a superheterodyne receiver. The millimeter wave part of the simplest superheterodyne receiver consists of an antenna, mixer, and local oscillator (LO). A millimeter wave signal is received with the antenna, and is down-converted from millimeter wave frequencies to intermediate frequencies (IF) using the mixer with the LO. The local oscillator is also used for the selection of the millimeter wave frequency down-converted to the IF. This kind of frequency selectivity is an important property, which has been used intensively, for example, in millimeter wave spectroscopy of H_2O and O_2, at 60 GHz, 118.75 GHz, and 183.5 GHz [38].

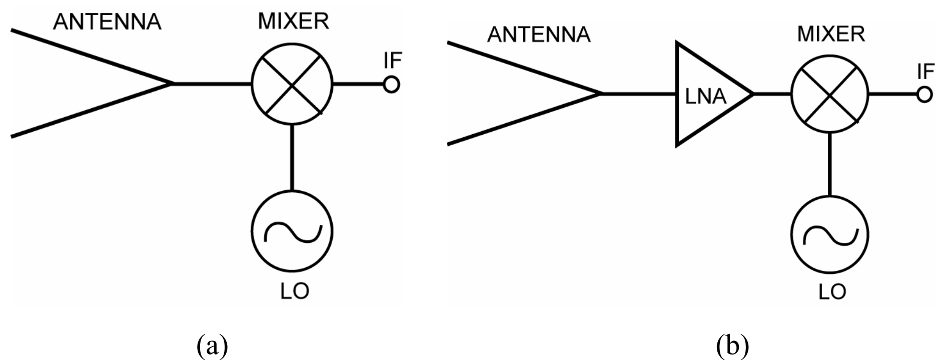

Figure 2. a) Schematics of a superheterodyne receiver, and b) a superheterodyne receiver with an LNA.

High stability low noise receivers used in advanced applications, like in the Planck mission, are more complicated than receivers in Figures 1 and 2 The Planck Surveyor has three channels at 30, 44, and 70 GHz in its low frequency instrument [42]. Figure 3 shows the schematics of these low noise receivers. The receiver front-end is cooled down to 20 K and the back-end is at 300 K. The receiver is based on direct detection, and it has about 60 dB gain.

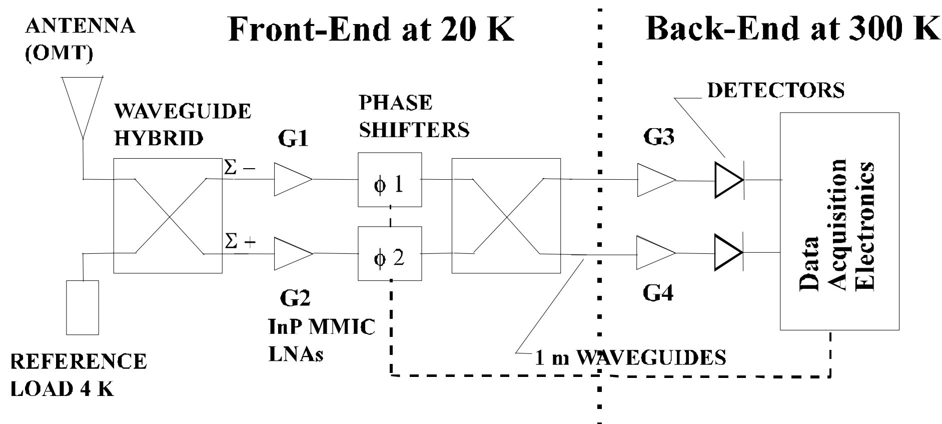

Figure 3. Schematics of low noise receivers used in the Planck mission at 30, 44, and 70 GHz [42].

Having low noise figure and high gain, low noise amplifiers are very important circuits in low noise receivers increasing their sensitivity. Currently, the use of

an LNA is beneficial before a mixer in low noise receivers up to about 200 GHz at room temperature and up to about 100 GHz at cryogenic temperatures [42]. Figure 4 shows a photograph of an LNA developed in the Planck Surveyor project. The LNA consists of four transistors. Cryogenic cooling lowers a temperature depended resistance in transistors thus lowering their noise figure and increasing their gain.

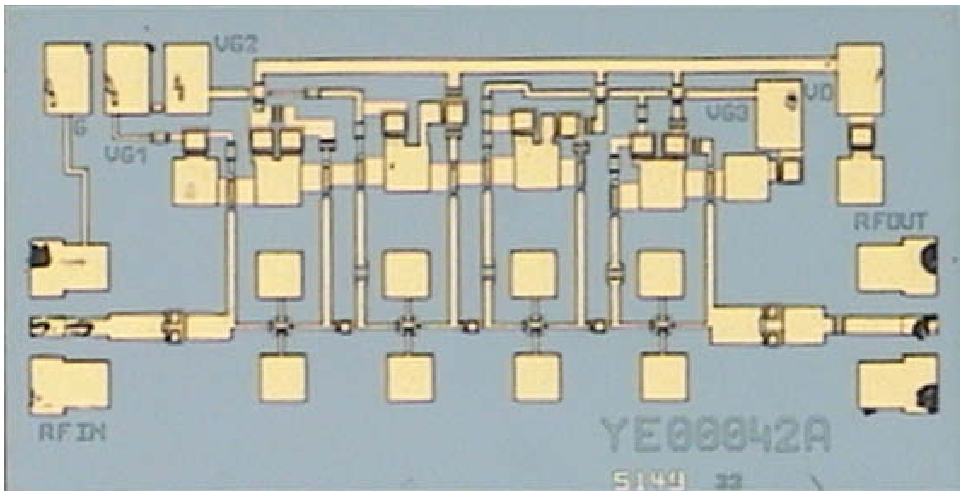

Figure 4. Photograph of a four-stage LNA developed in the Planck mission. The size of the chip is about 1.1 mm x 2.1 mm.

1.2 Research problem of this thesis

To design low noise amplifiers, models for transistors are needed. Transistors used in low noise amplifiers are treated as linear two-ports, and both the S- and noise parameters of the transistors are needed in the design of LNAs [43]. These can be obtained with simulations, but often on-wafer measurements are the most practical and accurate way to get them at millimeter wavelengths. After the design and fabrication of an LNA, its performance needs also to be measured, because it will be used as a part of a receiver. These measurements are usually done using on-wafer measurement methods. If LNAs are used in cooled cryogenic applications as in the Planck Surveyor, cryogenic on-wafer measurements are also needed both for transistors in the design phase and for fabricated LNAs in the receiver building phase.

The lack of commercially available on-wafer measurement systems for cryogenic and noise parameter measurements at W-band was the first practical research problem in this thesis work. Also, the level of measurement automation and accuracy could be increased with electrically controllable impedance tuners. To study suitable technologies and develop such integrated impedance tuners was the second research problem in this thesis work.

1.3 Scope and contents of this thesis

The focus of this thesis is on the development of on-wafer measurement techniques for millimeter wave device and circuit characterization as well as on the development of MEMS based circuits both for measurement and telecommunication applications. The research has been carried out at the Millimeter Wave Laboratory of Finland – MilliLab, VTT Technical Research Centre of Finland and at the Radiation Laboratory, University of Michigan, Ann Arbor, USA.

This thesis is divided into two parts: a summary and eight scientific articles. The summary gives introduction to the research area and results presented in the scientific articles. Introduction gives also a short introduction to low noise receivers, and shows how this thesis is connected to the low noise receiver development. In the summary, Chapter 2 discusses basic techniques related to on-wafer noise parameter measurements as well as on-wafer S-parameter measurements in cryogenic conditions. Chapter 3 gives introduction to integrated impedance tuners, presents several technologies used in impedance tuners, and compares existing integrated impedance tuners. Chapter 4 summarizes the work carried out in publications [P1–P8]. Both conclusions and future work are presented in Chapter 5.

Publications [P1, P2] and Chapter 2 present a cryogenic on-wafer S-parameter measurement systems for the 50–110 GHz frequency band, and noise parameter measurement system for W-band frequencies both developed in this thesis work. Both the S- and noise parameters of transistors needed in the LNA design can be measured with the measurement system. To improve on-wafer noise parameter measurement systems, MEMS based impedance tuners have also been developed in this thesis work. This development work is presented in Chapter 4

and publications [P3–P8]. Other publications related to this thesis work [1–5] present on-wafer measurement systems for transistor and LNA characterization. All these on-wafer measurement systems have been an important part of low noise receiver development at MilliLab as well as commercially available on-wafer measurement services provided by MilliLab.

1.4 New scientific results

This thesis has produced new knowledge and scientific results in the following areas:

1) cryogenic on-wafer measurements at millimeter wavelengths;
2) on-wafer noise parameter measurement methods and a system for W-band device characterization;
3) novel impedance tuners for measurement applications based on RF MEMS technology;
4) novel reconfigurable matching networks for telecommunication applications based on RF MEMS technology.

2. Millimeter wave on-wafer measurement techniques

On-wafer measurements are used for electrical characterization of components and circuits directly from a wafer or chip. On-wafer measurement techniques have been used in component characterization as long as integrated circuit techniques have been used in component fabrication. Component properties like DC-curves have been measured with needles already tens of years. Scattering (S-) parameter measurement is a basic tool in microwave and millimeter wave circuit characterization. The first wideband on-wafer measurement systems at microwave frequencies were presented at the beginning of 80's [44, 45]. Since that time, development work to extend on-wafer measurements to the millimeter wave frequencies have been carried out. Development has been driven mostly by scientific and military applications. On-wafer S-parameter measurement systems for W-band component and circuit characterization were presented in the beginning of nineties reaching 110 GHz [46–48]. In the late nineties and in the beginning of this century, on-wafer S-parameter measurements reached 200 GHz [48–51]. However, progress in on-wafer noise figure measurements has not been so fast. On-wafer measurement systems for noise figure and gain measurements at W-band have been published covering just part of the whole waveguide band [53–55]. For the first time, wideband 50–110 GHz on-wafer noise figure and gain measurements has been demonstrated in this work covering both the V- and W-bands [3]. In addition measurements over a wide frequency band, automated wafer scale measurements can be carried out with the developed measurement set-ups.

2.1 Cryogenic on-wafer measurements at V- and W-band

Especially in radio astronomical applications, active components and circuits are cooled down to low temperatures (10–100 K) in order to obtain as high performance as possible [8]. Also, on-wafer measurements are often the easiest and most straightforward way to get models for transistors and high temperature superconductor (HTS) devices at low temperatures and at millimeter wavelengths. For example, measured transistor models at cryogenic temperatures are needed in the design of cooled low noise amplifiers. Cryogenic on-wafer

measurement systems have been developed in other research groups mostly for frequencies below 50 GHz [56–58]. The first on-wafer measurement set-up for above 50 GHz for S-parameter measurements was developed at MilliLab [59]. In this thesis work, the V-band measurement system has been extended to W-band [1], and also, wideband 50–110 GHz cryogenic on-wafer S-parameter measurements of HEMTs have been demonstrated [P2, 5].

The developed cryogenic measurement system is based on a commercial cryogenic on-wafer system by Nagase Co originally designed for measurements below 50 GHz. The Nagase system consists of a stainless steel vacuum chamber, vacuum pump, cryocooler, cold plate (chuck) for the test devices, and a temperature controller. In addition to the Nagase system, a video microscope and a temperature monitor with four silicon diode temperature sensors have been acquired. All the installations necessary for waveguide based measurements above 50 GHz have been designed and built in-house.

The vacuum chamber has several feed throughs for both mechanical manipulators and electrical connections (Figure 5). Three of these are for RF and bias probe holders connected to xyz translation stages and one is for y-directional translation arm used for moving the chuck in that direction. The probes can be moved with the manipulators about the area of 25 mm x 25 mm. The probe holders are connected to a 10 K cold head with cold fingers. Two of the feed throughs have been built in-house for connecting WR-10 or WR-15 waveguides.

Inside the vacuum chamber, special in-house built spiral-shape metal waveguides are used for connecting the two feed throughs to the RF probes (see Figure 5). Each of the waveguides is about 450 mm long and consists of three sections. Two of the sections are gold-plated copper, and the third one is gold-plated stainless steel. The steel section is about 200 mm long, and it is provided for reasons of temperature isolation as well as mechanical flexibility. The feed throughs are in room temperature, whereas the device under test (DUT) can have a temperature as low as 15 K. The steel sections reduce heat flow to the DUT helping to maintain the wanted testing temperature. This flexibility of the steel sections makes it possible to adjust the positions of the RF probes.

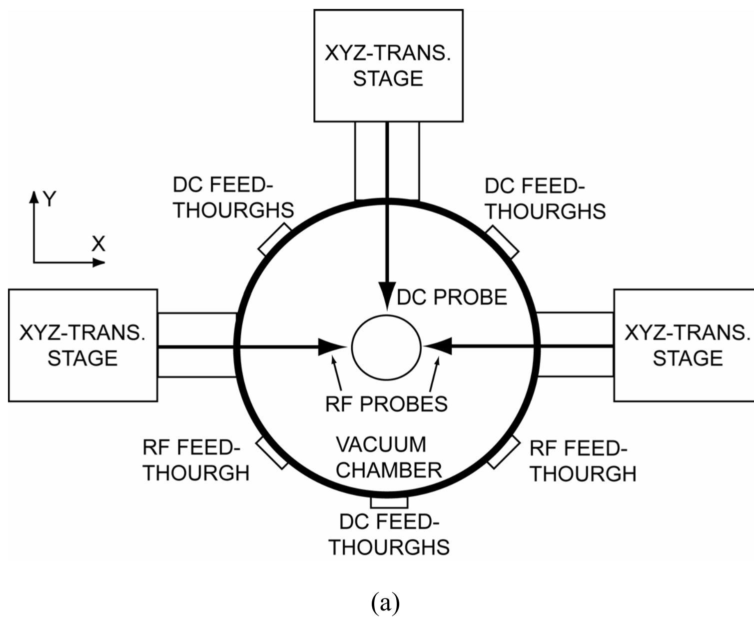

(a)

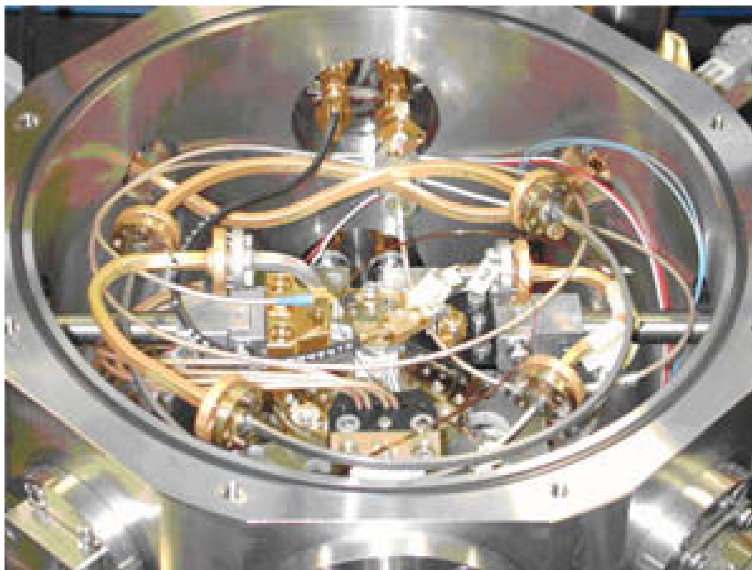

(b)

Figure 5. a) A schematic drawing of the cryogenic measurement station. b) A photograph showing the RF and bias probes with waveguide installations inside the vacuum chamber.

Publication [P2] describes the measurement systems and procedures for cryogenic on-wafer measurements at 50–110 GHz. The S-parameters of HEMTs (DaimlerChrysler and HRL) were measured at W-band and temperatures between 20 K and 295 K using the developed system [P2, 1]. HEMTs were also characterized in the 50–110 GHz frequency band and 20–295 K. Results showed good continuity between V and W-bands. For the first time, a cryogenic on-wafer measurement system and measurement results were presented at W-band and 50–110 GHz, being only published results for at this frequency range [1, 5, P2].

Error analysis for cryogenic S-parameter measurements was carried out in this work. Repeatability of on-wafer calibration and sensitivity for probe movements were investigated [5]. Repeatability of on-wafer calibration was moderate at W-band and good at V-band. The W-band measurement system was sensitive for x-directional probe movement, which caused the most significant errors. These errors were most probably due to the mechanical bending of the spiral waveguides. As a result of error analysis carried out in [5], the measurement system has been decided to be further develop. This includes the replacement of the spiral waveguides by straight waveguides to avoid bending of the waveguides.

2.2 On-wafer noise parameter measurements

Noise properties of a two-port can be presented using noise parameters. Noise parameters describe how the noise figure of the two-port changes as a function of source reflection coefficient. For example, noise figure of a HEMT varies as a function of source reflection coefficient. This is important information in the design of low noise amplifiers, because the LNA should provide a low noise figure and high gain at the same time.

The noise figure of a linear two-port as a function of source reflection coefficient Γ_i is given by [60]:

$$F = F_{\min} + \frac{4r_n}{1-|\Gamma_i|^2}\left|\frac{\Gamma_i - \Gamma_{opt}}{1+\Gamma_{opt}}\right|^2 \quad (1)$$

where F_{min} is the minimum noise figure of the two-port, r_n is the normalized (with reference impedance) noise resistance, and Γ_{opt} is the optimum reflection coefficient. Variables F_{min}, r_n and Γ_{opt} are called noise parameters. Graphical three-dimensional representation of Equation (1) in Figure 6 shows the noise paraboloid over the Smith chart. The minimum noise figure can be achieved with the optimum reflection coefficient.

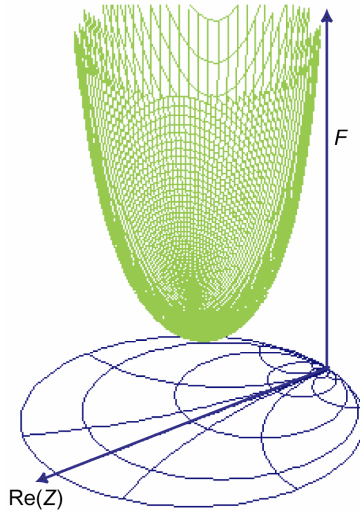

Figure 6. Graphical presentation of noise the figure paraboloid.

Noise parameters cannot be measured directly. In order to measure them, the input reflection coefficient of a device under test, DUT, is changed, and the corresponding noise figure of the DUT is measured. During late fifties and sixties, an experimental searching method for minimum noise figure and corresponding optimum reflection coefficient was used [61]. However, this method was found to be slow and inaccurate [62]. Alternatively, the noise figure paraboloid and noise parameters can be obtained by fitting Equation (2.1) to the measured data [62]. In order to do the fitting, the noise figure of the DUT should be measured at least with four different Γ_i values because Γ_{opt} is a complex quantity. Several methods have been developed for the noise parameter extraction purpose [62–66]. Lane's method [62] uses a least-squares data fitting technique, and it is used in this work [P1].

The schematics of a noise figure and traditional noise parameter measurement set-ups are shown in Figure 7 [61]. In noise figure measurements, a noise source producing two different noise temperatures is connected to the input of the device under test, and corresponding noise powers are measured with the noise receiver. This kind of measurement system is used for noise characterization with a 50-Ω reference impedance. In this work, similar systems have been used for wideband on-wafer noise figure and gain measurements of low noise amplifiers [2, 3, 5]. This kind of a set-up has also been used as a basis of the so-called F50 noise parameter extraction method [67–69]. The F50 method is a tunerless method, where wideband noise figure measurements are carried out, and transistors noise models are fitted to this data. These set-ups are simpler because impedance tuners are not needed but on the other hand, wideband measurements are necessary as well as accurate noise models for transistors. Suitability of the F50 method for noise characterization and modeling purposes has also been criticized due to the lack of accurate noise models at millimeter wavelengths [70].

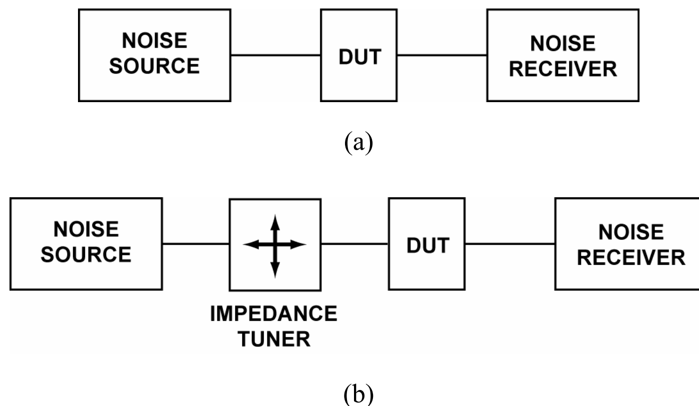

Figure 7. Schematics of a) noise figure measurement system and b) traditional noise parameter measurement system.

The traditional noise parameter measurement system has an impedance tuner between the noise source and DUT in order to generate impedances differing from 50-Ω (Figure 7b). The loss of the two-port tuner increases at the same time when the magnitude of the reflection coefficient is increased. This is problematic because the noise power delivered to DUT is reduced lowering the measurement accuracy [71].

Improved measurement systems for noise parameter measurements are shown schematically in Figure 8. These systems are based on the cold-source method, because the noise source is used here only for the calibration of the noise receiver, and is not needed for the noise measurements of DUT [71–73]. If the noise source is at the input side of DUT (Figure 8a), the device under test is replaced with thru connection in receiver calibration. If the noise source is at the output side of DUT (Figure 8b), then just a switch is needed to connect the noise source to the noise receiver. The later method is used in this work [P1].

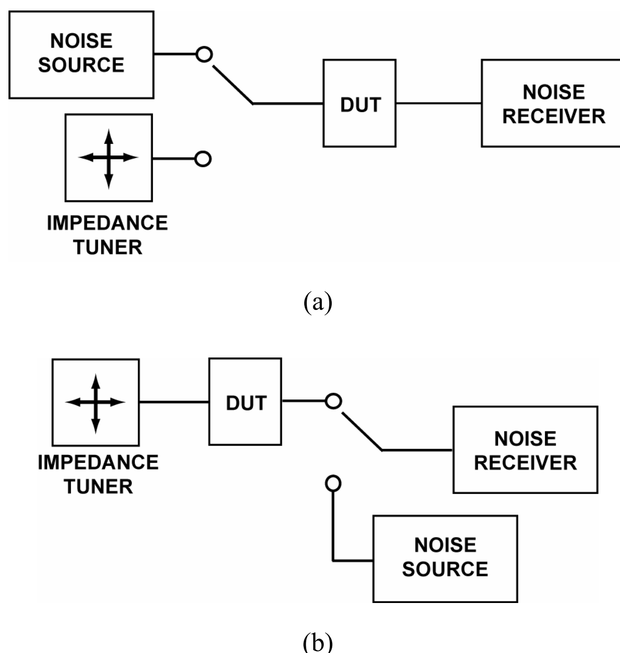

Figure 8. Schematics of the cold-source measurement set-ups for noise parameter measurements.

Waveguide based (WR-10) on-wafer measurement set-up used in this work is presented schematically in Figure 9 [P1, 6]. Also, the reference planes A, B, C, D, and E are shown there. DUT is connected to the measurement system using waveguide probes. By including two waveguide switches, both noise and S-parameter measurements can be done without breaking any connections. Only a simple uncalibrated 1-port impedance tuner is needed at the input side of the device under test. This is possible due to the switch 1. The 1-port tuner consists of an adjustable waveguide backshort and attenuator. System characterization

and the S-parameter measurements of DUT are done using a HP8510C vector network analyzer. Also, the VNA is needed during noise measurements of DUT to measure the reflection coefficient of the impedance tuner. The noise source is used here only during the calibration of the noise receiver. The noise receiver calibration can also be done during long measurement sessions without breaking any connections due to the switch 2. An LNA is used for increasing the sensitivity of the noise receiver. The LNA was obtained through the Planck Surveyor collaboration [8]. The mixer is used for downconverting the noise power from W-band to the measurement region of a HP8970A noise figure meter. The local oscillator (LO) chain consists of a HP83650A synthesized sweeper, HP8349B microwave amplifier, and HP83558A mm-wave source module. All measurement instruments are controlled using a PC via GPIB line. The PC and in-house written software make automatic data acquisition and complex calculations possible.

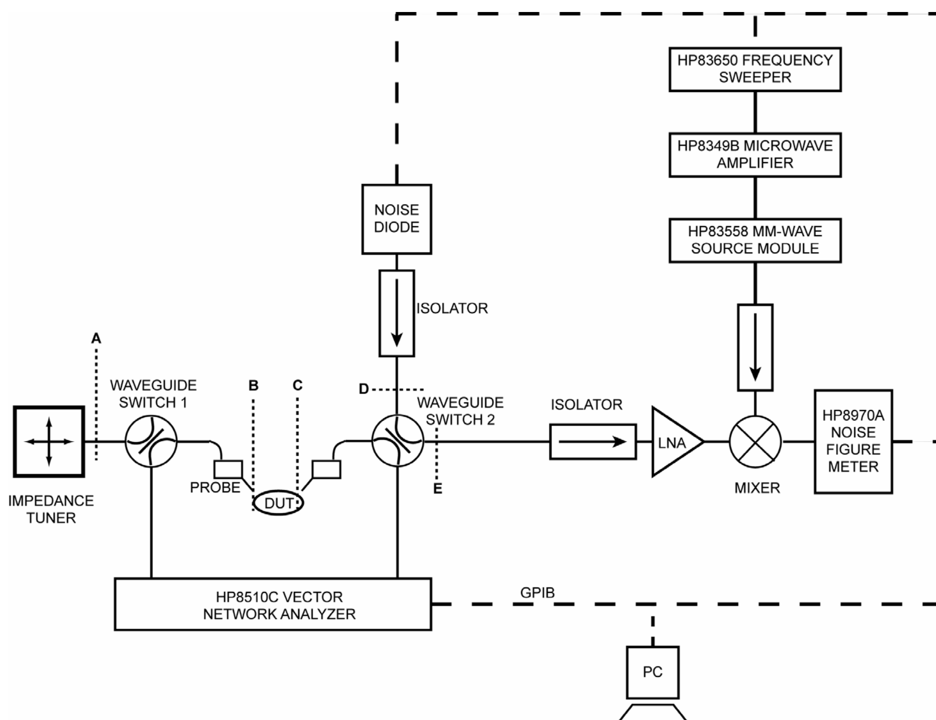

Figure 9. Schematics of the W-band on-wafer measurement system used in this work. Reference planes A, B, C, D, and E are also shown [P1].

On-wafer noise parameter measurements consist of several steps as shown in Figure 10. In system characterization, both waveguide and on-wafer calibrations are needed. To characterize the noise receiver, the noise source is connected to the noise receiver as in Figure 9. After this, the S-parameters of the device under test are measured. At this point, the VNA is calibrated to the reference planes B and C using on-wafer calibration. Typically, on-wafer Line-Reflect-Reflect-Match (LRRM) [74], Short-Open-Load-Thru (SOLT) [75], or Thru-Reflect-Line (TRL) [76] calibration method is used at MilliLab. The first step in actual noise measurements of DUT is to set suitable source reflection coefficient with the manual tuner. At that time, the tuner is switched to the VNA so that the reflection coefficient can be set and measured with the VNA. After this, the tuner is switched to DUT and corresponding noise power is measured with the noise receiver. The two latest steps are repeated for all different tuner positions. All these steps need to be done at all frequency points of interest. Finally, complicated calculation routines are performed and noise parameters are calculated. In this work, data analysis, calculation routines, and statistical analysis were done with self-written programs in Matlab[1].

[1] Matlab is a product of Mathworks, www.mathworks.com

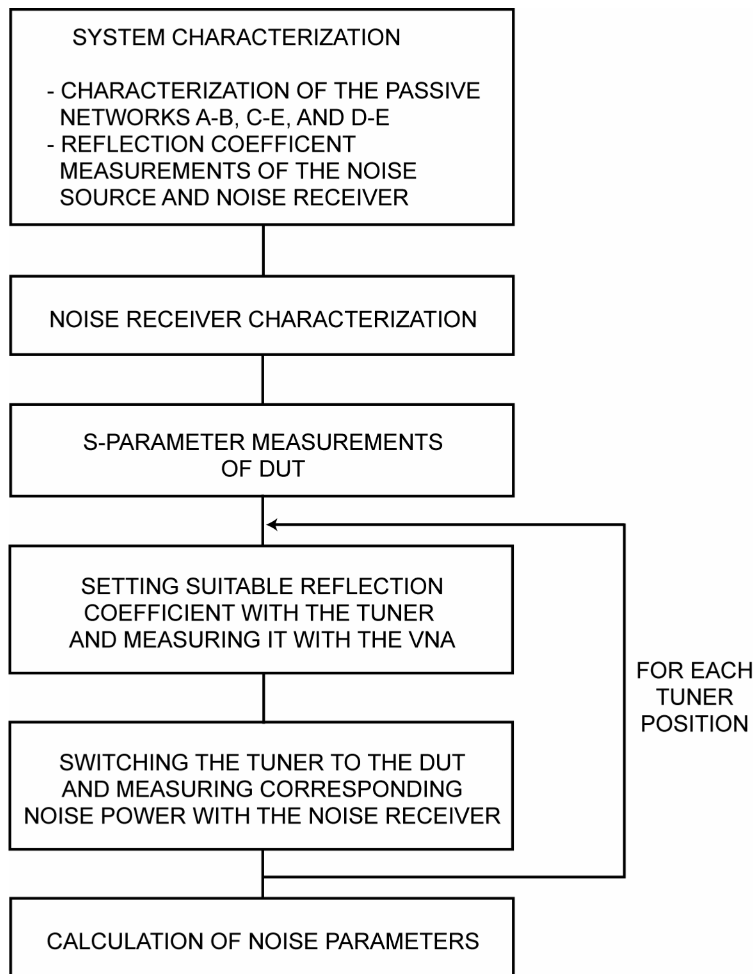

Figure 10. Measurement flow for noise parameter measurements.

Only a few noise parameter measurement results have been published for frequencies above 50 GHz. Webster et al. have presented noise parameter measurement results at V-band up to 60 GHz in coaxial systems [77], and V-band on-wafer noise parameter measurement systems and results have been published only by researchers from MilliLab [72–74]. Lahdes et al. have developed measurement system based on the cold source method and uncalibrated manual impedance tuner in MilliLab [78–80]. Kantanen et al. have developed wideband automated on-wafer measurement system for V-band noise parameter measurements, which uses commercial motorized V-band impedance tuner [4]. Before this work, only single frequency on-wafer noise parameter

measurement results have been published at W-band by Alam et al. and only for a passive device [81, 82]. Measurement results presented in this work are unique, being the only published wideband results at W-band.

In this work, an on-wafer noise parameter measurement set-up has been developed for W-band device characterization. Detailed description of the developed measurement system and procedures has been given. The noise parameters of an InP HEMT (DaimlerChrysler 2 x 40 μm) have been measured, and measurement results have been presented in 79–94 GHz frequency band. A similar device has been measured at V-band [4], and good agreement has been reached between the measurements [P1, 5]. It has also been shown in this work that wideband measurements are often the best way to find out possible errors in measurements of active devices [P1, P2, 2–5]. Especially, if measurements are carried out with different set-ups and at several frequency bands, possible measurement errors can be more easily identified. Also, wideband fitting can be done to the wideband results in order to get better models for devices.

The measurement set-up can be further improved to get more wideband results, and also the automation of the set-up can be increased. A drawback of the current W-band noise parameter measurement set-up is that the measurements are done manually, because of the manual impedance tuner. This requires presence of a person at all times during the measurements. To improve the measurement system, an automated W-band impedance tuner would be needed. This kind of automated measurement set-up based on a motorized impedance tuner has been successfully developed at MilliLab by Kantanen et al. for wideband on-wafer noise parameter measurements at V-band [4]. More detailed development plans for integrated impedance tuners are given in the next chapter.

3. Reconfigurable RF MEMS impedance tuners and matching networks

A manual impedance tuner is currently used in the W-band on-wafer noise parameter measurement system (Figure 11) [P1]. Currently, the tuner consists of an adjustable waveguide backshort and attenuator, and high reflection coefficients can be produced with such a tuner. However, the maximum reflection coefficient that can be obtained at the probe tip (reference plane B in Figure 8) is limited by the loss of the passive network between the impedance tuner and device under test. In practice, the maximum reflection coefficient that can be reached with the set-up at the probe tip is from 0.7 to 0.72 depending on the frequency.

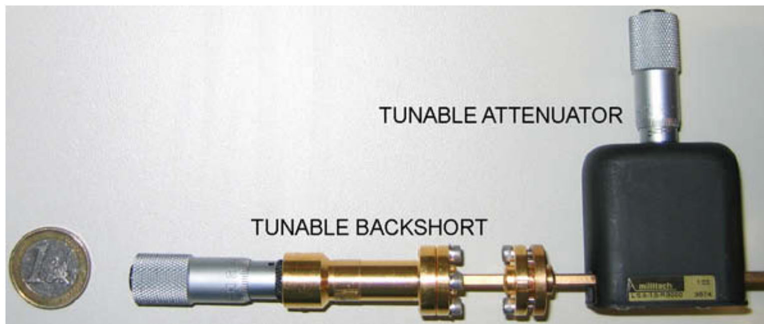

Figure 11. Manual impedance tuner used in W-band noise parameter measurements consisting of an adjustable waveguide backshort and attenuator.

A commercial motorized impedance tuner is used in a V-band on-wafer measurement set-up at MilliLab [4]. Similar tuners have also been developed for W-band systems [83]. Step motors are used for moving a probe inside a waveguide in the tuner thus changing the tuner output impedance. It is evident that the level of measurement automation can be increased with a motorized tuner. A further step would be to develop an electrically controllable impedance tuner packaged into a waveguide split-block, and a size comparison between the motorized impedance tuner and the waveguide split-block is shown in Figure 12. The size of the motorized impedance tuner is about 110 mm × 125 mm × 130 mm with a weight of about 0.5 kg. In comparison, the waveguide split-block is quite small (12 mm × 15 mm × 20 mm) and is easy to use with coplanar probes and

probe stations in on-wafer measurement systems. The maximum achievable reflection coefficient, $|\Gamma_{MAX}|$, which can be generated using waveguide tuners, is very high (about 0.97) but this is referred to the tuner output. For on-wafer measurements, the loss of the connecting waveguide sections and RF probe can limit $|\Gamma_{MAX}|$ to about 0.7–0.8 at 50–110 GHz [4, P1]. Despite the size benefit of an integrated tuner inside the split-block, the maximum reflection cannot be increased significantly because the probe still remains between the tuner and DUT. A major improvement would be to place an integrated tuner inside a measurement probe. In this case, the loss between the tuner and DUT could be minimized. This is shown schematically in Figure 13.

Figure 12. A photograph of a motorized waveguide impedance tuner and a waveguide split-block.

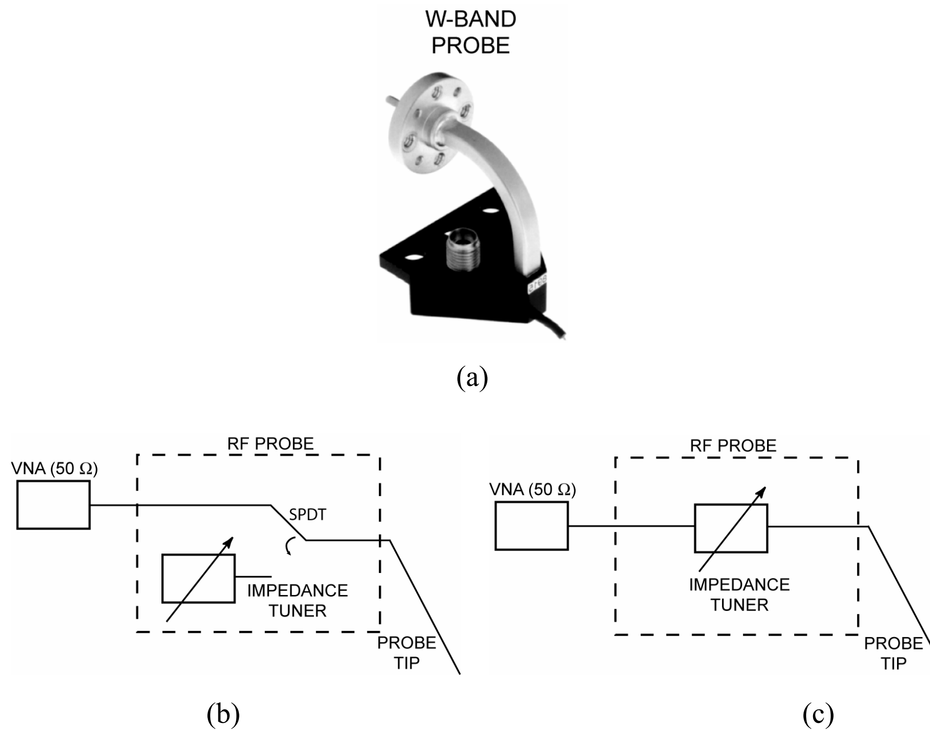

Figure 13. a) W-band on-wafer measurement probe[2], b) schematics of a reflection, and c) a transmission type impedance tuner inside a probe.

In addition to measurement applications, impedance tuners can be used in telecommunication and defense applications for reconfigurable matching networks or impedance tuners. Reconfigurable matching networks are beneficial in multi-band and reconfigurable systems. Figure 14 presents a conventional and reconfigurable multi-band front-end. Portable handsets already use multiple frequency bands since they need to be functional on many continents with different frequency allocations. Also, the number of frequency bands is expected to increase in the near future because new applications (GPS, WLAN etc.) are being integrated into handsets. Also at microwave and millimeter wave frequencies, radio links are using many different frequency bands including bands around 7, 8, 13, 15, 18, 23, 26, 28, 38, 42, and 58 GHz, and reconfigurable circuits would allow the radio to operate at several bands.

---

[2] www.ggb.com

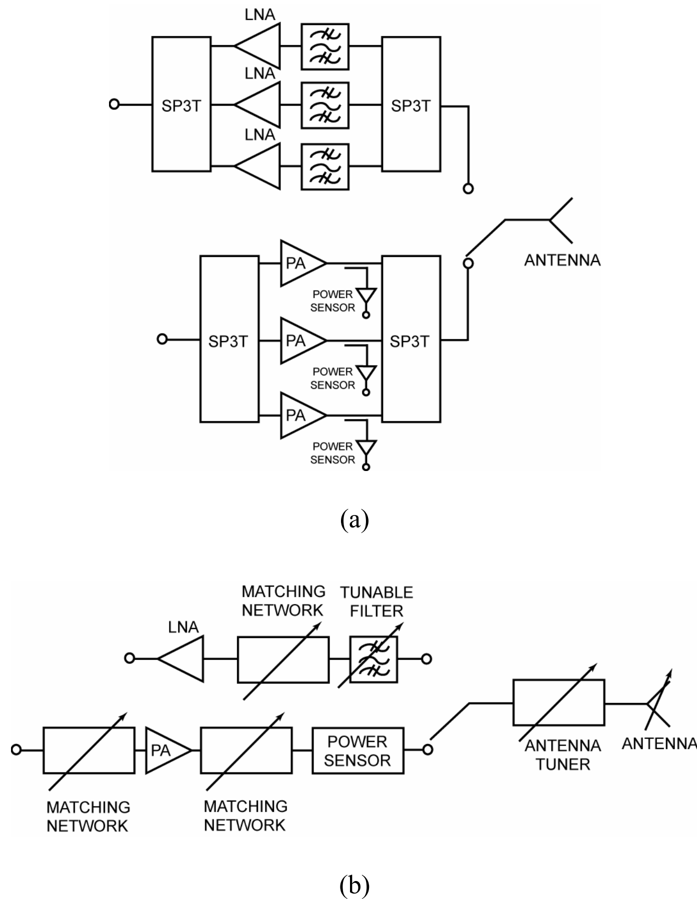

(a)

(b)

Figure 14. a) Conventional and b) reconfigurable multi-band front-end.

Other types of problems, existing both in single- and multi-band systems especially in mobile phones, are proximity effects. A typical situation is that a user places a mobile phone next to his head during a call (Figure 15). In this case, the antenna resonance frequency is shifted due to near-field coupling with the human head resulting in an impedance change at the operation frequency. This also creates a mismatch between the power amplifier (PA) and the antenna, thus reducing the output power. These effects could be decreased using a reconfigurable matching network between the PA and the antenna or using an antenna tuner inside the antenna to maintain the same resonance frequency. Mobile phone antennas with antenna tuners based on transistor switches are already commercially available, and their use is expected to increase in the near future due to the of multi-radio phones.

Figure 15. When a person uses his mobile phone, the performance of the mobile phone front-end is changed because the phone is next to the head.

Specifications for impedance tuners depend on the application. In noise parameter measurements, transmission loss is not very critical but it is beneficial to have a good impedance coverage over a wide frequency range, and these impedance tuners can be both reflection and transmission-type circuits (see Figure 13). On the other hand, matching networks and antenna tuners should have as low loss as possible still producing impedances needed in changing matching conditions. In most cases, matching networks and antenna tuners are transmission type circuits. These components should also have good RF power handling capabilities in case they are used with power amplifiers. Furthermore, linearity is one of the most important properties in receiver or transmitter applications, and it is important that the reconfigurable circuits produce very little additional distortion. This chapter presents several topologies and realizations for integrated electronically controllable impedance tuners.

3.1 Tuner topologies

3.1.1 Stub-based impedance tuners

Stub-based matching networks are mature matching technology in microwave and millimeter wave applications, especially in coaxial implementations [84–87]. Lumped element tuners and matching networks can be used at frequencies below 6 GHz. Also, integrated-circuit technologies have made possible to realize stubs with integrated capacitors and inductors at microwave frequencies. Stub matching networks are quite narrowband circuits, because the lengths of stubs and distances between them are proportional to the wavelength. They can be made tunable by using screws, tunable backshorts, and other tuning elements. In this work, emphasis has been in the development of reconfigurable electrically controllable integrated impedance tuners for several frequency bands. Standard single-, double-, or triple-stub matching networks can be made tunable by integrating tuning elements into these circuits. Next, some possible stub-based impedance tuner topologies are shown, and several tuning methods are presented.

Stub topologies

Stub-based impedance tuners/matching circuits are based on single-, double-, or triple-stub topologies [84]. In order to make the stub-circuits tunable, the electrical length and/or impedance of the stubs needs to be tuned. The sections between stubs can also be tunable for achieving wider impedance coverage. Figure 16 presents some possible stub-based impedance tuner topologies. Parameters L_1, L_2, L_3, L_4, and L_5 are the electrical lengths of the stubs and sections between them, meaning that their electrical length as well as their impedance can be tuned.

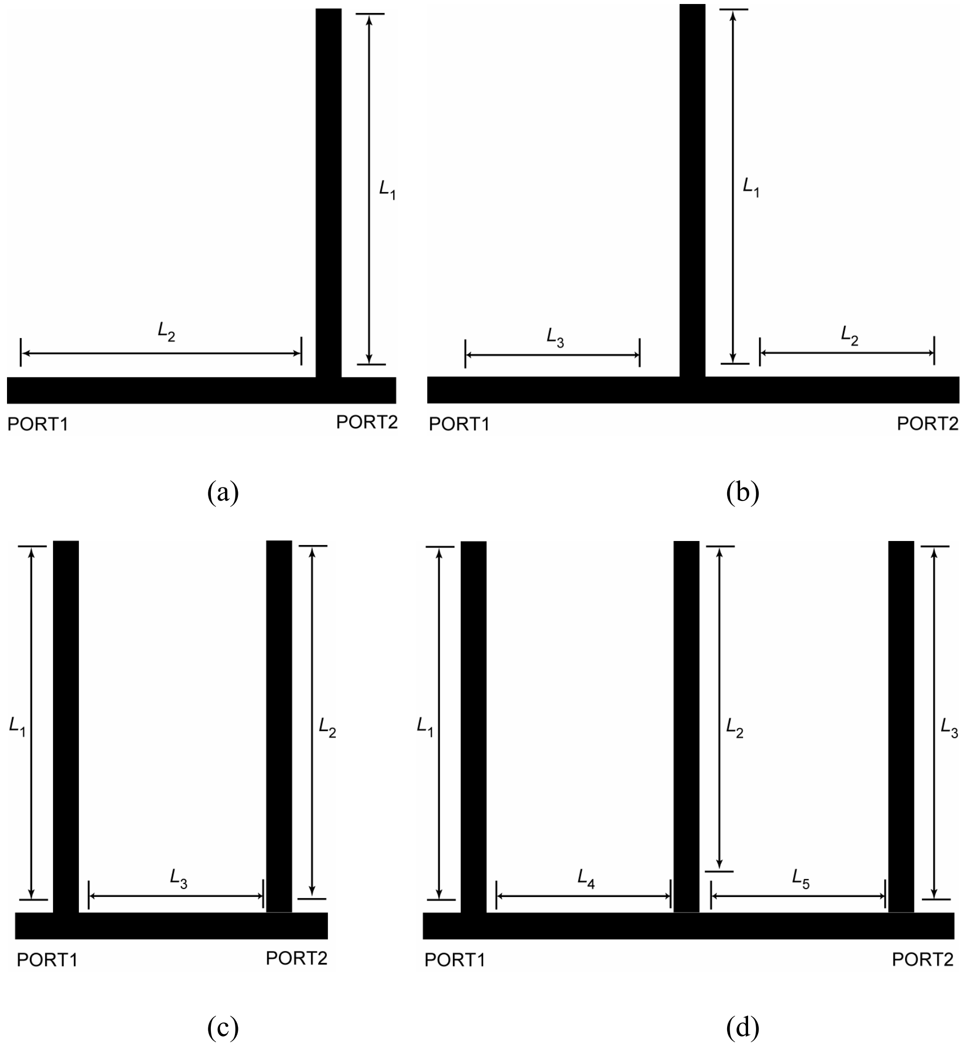

Figure 16. Tuning the electrical lengths of the stub-based circuits.

Tuning methods

Tuning possibilities are divided here into two main categories: digital and analog tuning. Digital tuning means that impedances are generated in a discrete manner using, for example, switches or capacitor banks with several fixed capacitances. Analog tuning is a continuous tuning which is realized, for example, with varactors having continuous tunability. Some possible analog and digital tuning

methods for changing the electrical length and/or impedance of stubs are shown in Figures 17 and 18, respectively [87].

By having a capacitor bank (Figure 17a) or a varactor (Figure 18a) at the end of the stub, the electrical length of the stub can be tuned. Also, the impedance of the stub is changed locally in the end of the stub because of increased capacitive loading. An other way to realize analog tuning (both electrical length and impedance), is to distribute many varactors along stub allowing larger tuning compared to just a single varactor at the end of the stub (Figure 18b). Also, stubs with different lengths or impedances can be switched to provide different impedances (Figure 17b and c). Straightforward methods for controlling the electrical length of the stub are to use series switches to connect transmission line sections (Figure 17d) or movable short circuit realized with switches in this case (Figure 17e). Both the electrical length and impedance of the stub can be controlled simultaneously with switched capacitor-based loading (Figure 17f).

If the capacitor bank at the end of the stub (Figure 17a) is realized with three switches then $2^3 = 8$ (2^N impedances, N = number of switches) different impedances can be generated. In thus case, the total loading capacitance is $C_{TOT} = 0$, C_1, C_2, C_3, C_1+C_2, C_1+C_3, C_2+C_3, or $C_1+C_2+C_3$. The same amount of different impedances (2^N) can be generated also with the designs in Figures 17b, c, and f. Designs in Figures 17 d and e produce N+1 different impedances. The difference between the two methods, 2^N vs. N+1 impedances, becomes significant if a larger amount of switches is used. For example, if N = 8, then the first type of tuning produces 256 impedances and the latter only 9 (this assumes that capacitances should be chosen correctly in the first type of tuning). In theory, unlimited number of impedances can be generated using analog type tuning as in Figure 18. However, this tuning range is limited in practice by the tuning range of a single varactor, parasitics of the varactors, and the number of varactors used. Also, the loss of the circuit is increased when the number of tuning elements in increased. This reduces the maximum available reflection coefficient.

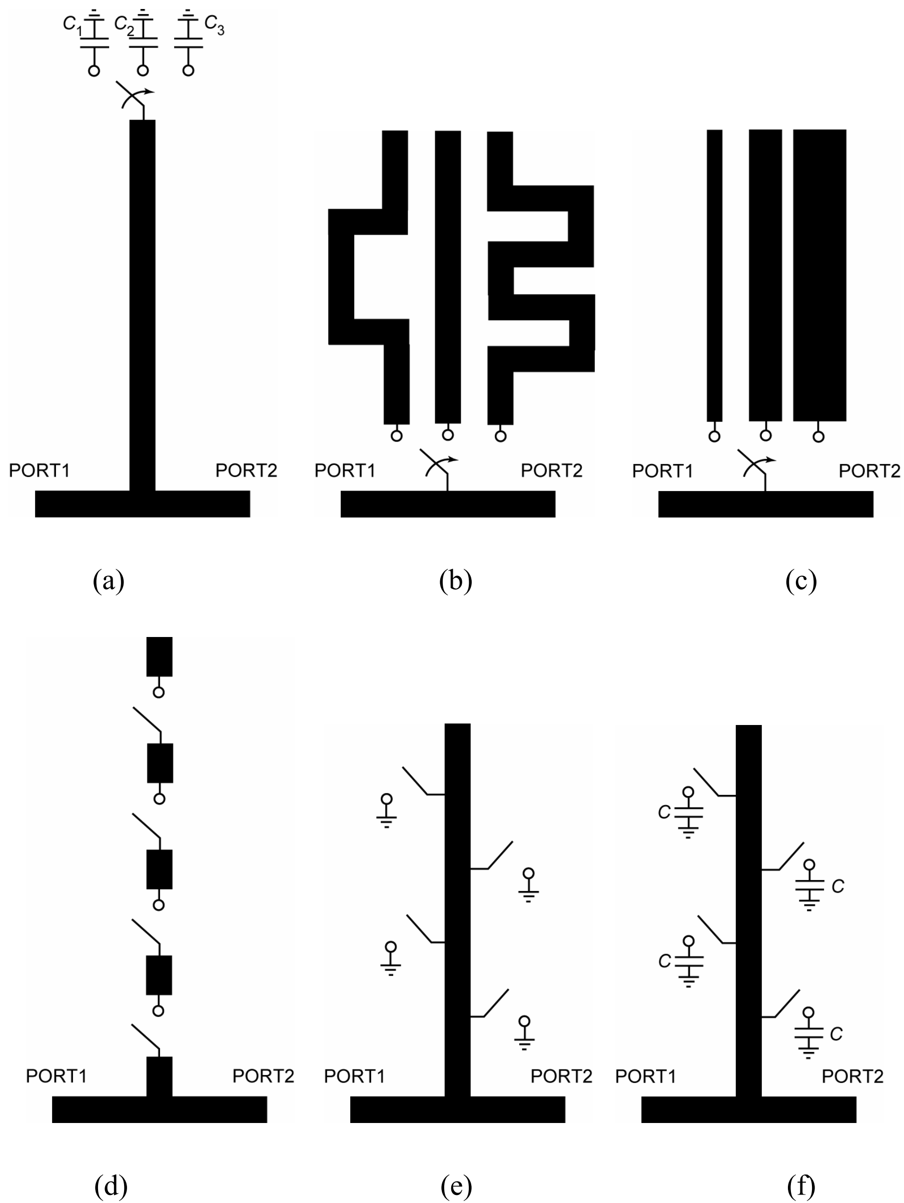

Figure 17. Electrically tunable stubs with digital type tuning. Tuning realized with a) capacitor bank at the end of the stub, b) switchable stubs with different electrical lengths, c) switchable stubs with different transmission-line impedance, d) series switches in a stub for different stub lengths, e) shunt switches in a stub for different stub lengths, and f) switched capacitors in a stub.

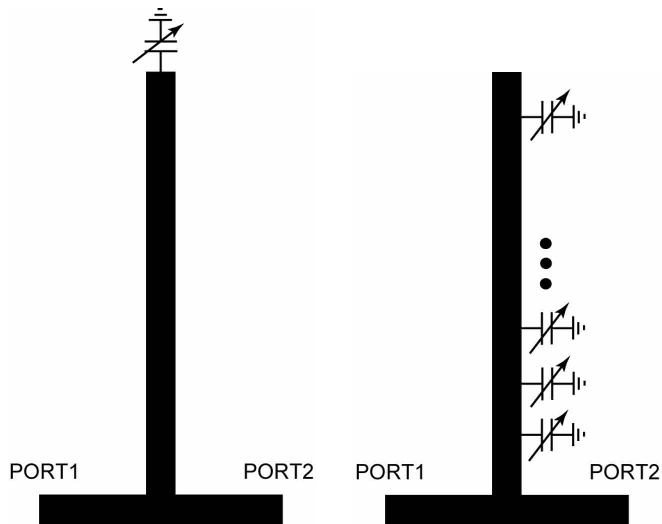

Figure 18. Electrically tunable stubs with analog type tuning. Tuning realized with a) a varactor in the end of the stub and b) many varactors distributed along the stub.

The electrical distance between the stubs and the impedance of these sections can be controlled electrically to increase impedance coverage of a tuner, and the same tuning methods which are used with stubs can be applied to sections between, before, and after the stubs.

Just some possible solutions for tuning have been shown here. By combining topologies shown in Figure 16 to tuning methods in Figures 17 and 18, several new impedance tuners can be realized. New tuners can be created easily using innovative stub structures as in [88–90]. Also, by coupling or connecting stubs together in the double- or triple-stub topologies, novel tuners can be developed. The most limiting factors in impedance tuner design are probably imagination and creativity of designers.

3.1.2 Slug tuners

Double-slug tuners have been used for a long time in coaxial systems [84]. Figure 19 shows the principle of the double-slug tuner topology two movable short circuits or sections having different impedance from the transmission line

impedance. By changing the distance between the short circuits or impedance sections (L_2) and distance from the port 1 (L_1), different reflection coefficients can be generated. Maximum reflection coefficient is defined by the impedance ratios between the transmission lime impedance and impedance section having the highest value in the case of the short circuit.

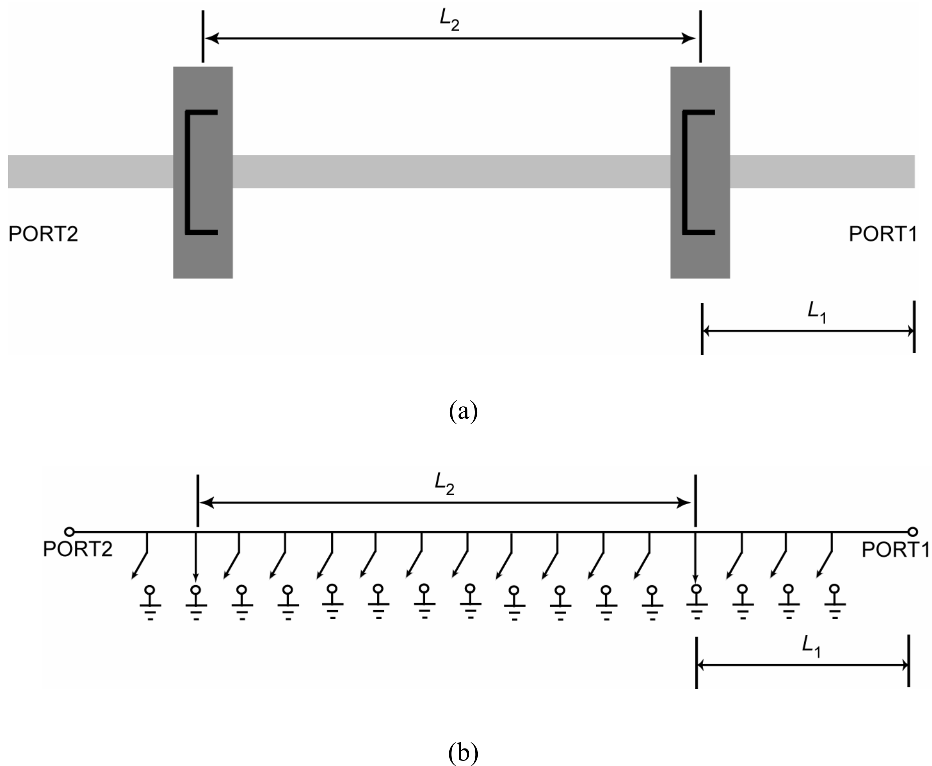

Figure 19. a) Schematic drawing of a double-slug tuner. b) Electrically tunable short circuits realized with switches.

3.2 Components for electrically controllable impedance tuners

3.2.1 Varactor diodes and transistors

All topologies presented above can be realized with active devices such as transistors or diodes. Active devices based on diodes and transistors can be used

as switches, or their capacitance can be changed as in varactor diodes. Their benefits are, at least, that the technology of active devices is already well established and tens of foundries exist for the fabrication of MMICs. Also, they have a low control voltage (0–10 V), they are fast (ns), produce gain (transistors only), and integration of other circuits like LNAs, PAs, mixers, and multipliers is possible in the same process. However, they also have several drawbacks when used in impedance tuners and matching networks. The best performance active devices at millimeter wavelengths are based on Indium Phosphide (InP) processes which are very expensive. Also, active devices generate noise and non-linearities, decreasing the system performance. The generation of noise and nonlinearities is problematic for applications in systems before the large gain stages, such as tuning for antennas and amplifier input matching. From the impedance tuner point of view, the biggest disadvantage of millimeter wave diode varactors is their quite high resistance [91] being lossy and limiting available impedance coverage. Noise can cause problems in noise parameter measurements, because any unwanted noise coming from the measurement system should be minimized to avoid additional calibration steps.

3.2.2 MEMS switches and varactors

MEMS technology offers the possibility to use mechanically movable micro scale elements that can be controlled electrically in microwave and millimeter wave applications. MEMS technologies have been applied to accelerometers and sensors (pressure, gas, and temperature) already from 1970s, and several commercial products have been available since the early nineties. The first MEMS switch and varactor for microwave applications have been presented in 1991 [92]. MEMS technologies have been applied to microwave and millimeter wavelengths mostly after 1995, and packaged MEMS switches are commercially available from several companies such as Radant MEMS[3], Teravicta[4], and Magfusion[5]. An extensive introduction and also, deep analysis of RF MEMS technology, components and circuits can be found in [87]. In this thesis work,

---

[3] www.radantmems.com

[4] www.teravicta.com

[5] www.magfusion.com

capacitive MEMS switches are used. In addition to the capacitive MEMS switch, other kinds of switches are also used in other research groups. Especially DC metal-to-metal contact switches are used in many applications below 5 GHz. Commercially available MEMS switches by Radant MEMS, Teravicta, and Magfusion are metal-to-metal contact switches.

Capacitive MEMS switches and varactors

Figure 20 shows one possible layout and schematical cross-sectional view for a capacitive shunt switch. This is very similar to a standard air bridge used in integrated circuits, but with a movable bridge.

If a voltage is applied between the CPW center conductor (signal) and ground, the bridge starts to curve towards the signal line. From the electrical point of view, this means that the capacitance between the CPW signal and ground is changed. If the voltage is increased, then the bridge collapses to the down-state position, also called "pull-down". Pull-down occurs, when the distance between the bridge and the signal line is reduced to 2/3 of its original distance [81]. The Voltage needed to pull-down the bridge is called pull-down voltage and is:

$$V_p = \sqrt{\frac{8k\delta^3}{27\varepsilon_0 A}} \tag{2}$$

where k is the spring constant of the bridge, ε_0 is the permittivity of vacuum, A is the overlapping area of the electrodes, and δ is the distance (gap) between the electrodes.

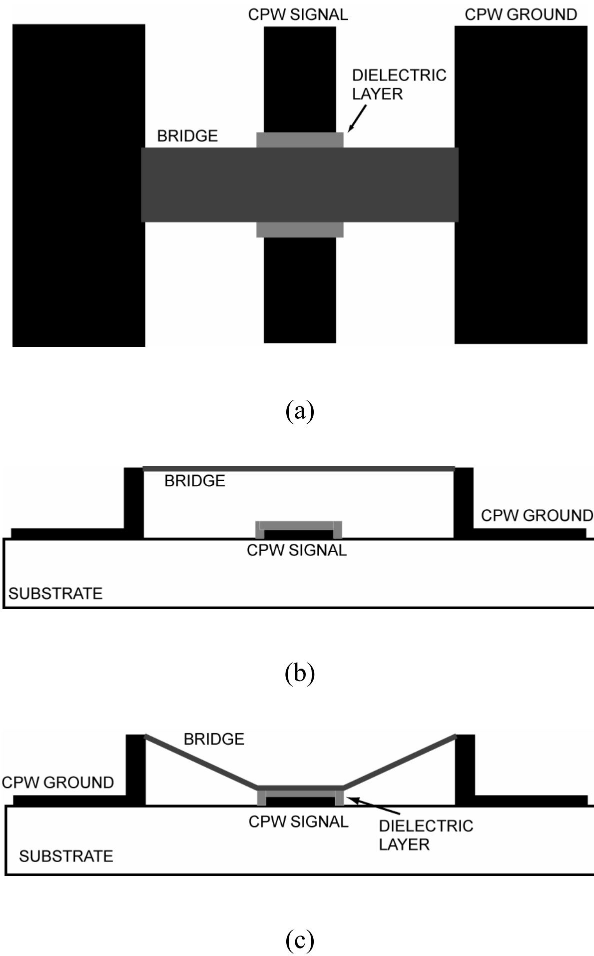

Figure 20. Shunt switch in a CPW configuration: a) top view, b) side-view in the up-state, and c) side-view in the down-state. The size of a MEMS bridge (switch) used in [P3, P7] is 80 $\mu m \times 280$ μm.

Capacitance of a MEMS switch or varactor can be calculated approximately with the parallel-plate capacitor equation

$$C_{\mathrm{MEMS}} = \frac{\varepsilon_0 \varepsilon_{\mathrm{r}} A}{\delta} \quad (3)$$

where ε_r is the relative dielectric constant of the material between the electrodes. A thin dielectric layer is used for covering the bottom electrode of a MEMS

switch to get high down-state capacitance and prevent DC contact between the electrodes (Figure 20). The previous equation can be used for calculating both the up and down-state capacitances approximately. If it is used in the down-state, then δ and ε_r are the thickness and relative dielectric constant of the dielectric layer. In practice, the actual up-state capacitance is 20–40 % higher than calculated from Equation (3) due to fringing fields.

The capacitance ratio of a capacitive MEMS switch between the up and down-states is typically between 20–100 depending mostly from the gap, δ, thickness of the dielectric layer, quality of the dielectric layer, smoothness of all layers, and contact force between the surfaces in the down-state [87, 94–98].

Equivalent circuits for a MEMS switch or varactor is shown in Figures 21 and 22, where R_{MEMS} and L_{MEMS} are the resistance and inductance of the MEMS component, and Z_0, β, and l are the transmission line impedance, propagation constant, and length, respectively.

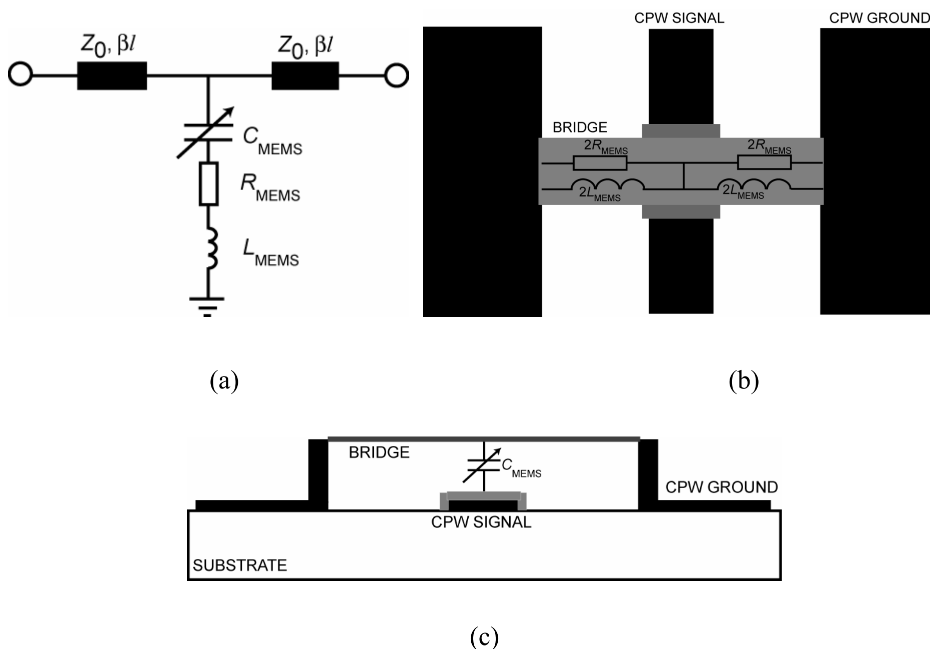

Figure 21. a) Equivalent circuit of capacitive shunt switch or varactor. Schematical drawing of a shunt switch showing the physical meaning of the equivalent circuit. b) Top view and c) side view.

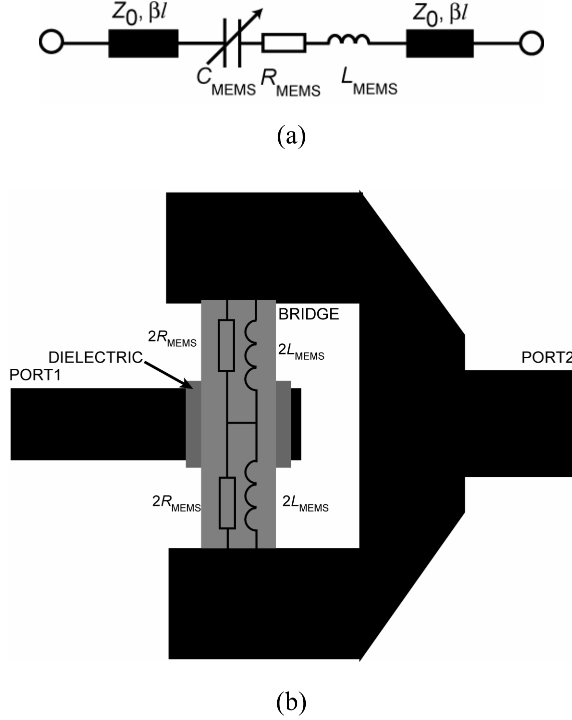

Figure 22. a) Equivalent circuit of a capacitive series switch and b) its possible layout.

The bridge can be used also as an analog varactor because the gap between the electrodes can be changed about 1/3 before the bridge pulls down. This method has been applied successfully to many tunable circuits like phase shifters [25] and filters [99], but has a limited capacitance ratio of only 1.4.

Switched capacitors

The capacitance ratio (20–100) and down-state capacitance of a MEMS switch is too high for many tunable and reconfigurable circuits. The capacitance ratio and down-state capacitance can be lowered by using fixed capacitors with smaller capacitance in series with the MEMS switch (Figure 23). The total capacitance of the switched capacitor is a series combination of the fixed capacitor and the capacitance of the MEMS switch:

$$C_{\mathrm{TOT}} = \frac{C_{\mathrm{MEMS}} C_{\mathrm{FIXED}}}{C_{\mathrm{MEMS}} + C_{\mathrm{FIXED}}} \tag{4}$$

In this case, the up-state capacitance is mostly defined by the up-state capacitance of a MEMS switch and the down-state capacitance by the fixed capacitor. Depending on the needed capacitances, fabrication process, and frequency, the fixed capacitors can be realized with stubs [100], metal-air-metal (MAM) [101], or metal-insulator-metal (MIM) capacitors [102]. If microstrip transmission lines are used, then stubs can be more easily implemented than MAM or MIM capacitors (all of these can also be applied to CPW circuits). The capacitance of MAM or MIM capacitors can be calculated easily with the parallel-plate capacitor equation. An additional advantage is that MEMS switches can be DC separated from other parts of circuits with the fixed capacitors.

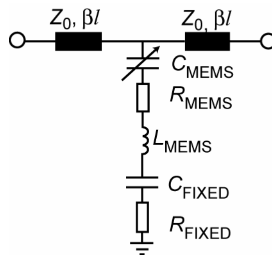

Figure 23. Equivalent circuit of a MEMS switch in series with a fixed capacitor.

The work in this thesis is primarily based on switch capacitors. These were realized with MEMS switches in series with MAM capacitors [P3–P8]. Figures 24 and 25 show the equivalent circuit and photograph with a cross-sectional view of a switched capacitor used as a tuning element in [P4]. Similar switched capacitors with different dimensions were also used in this work up to 80 GHz [P3, P6, P7, P8]. The fixed metal-air-metal capacitor is formed the following way: the bottom electrode of the MAM capacitor is the continuation of the MEMS switch and the top electrode is realized with the thick electroplated CPW ground. This can be made easily from the fabrication point of view. The same sacrificial layer is used under the MEMS switch and MAM capacitors, and it is removed later on. The capacitance of the MAM capacitors can be controlled accurately since the sacrificial layer thickness is controlled within ±0.1 μm. By changing the area of the MAM capacitor, the capacitance ratio and down-state capacitance of the switched capacitor can be chosen to be any value as long as it is less than the capacitance ratio and the down-state capacitance of the MEMS switch itself. In this particular case, the capacitance ratio of the switched capacitor was chosen to be 2.5 [P4].

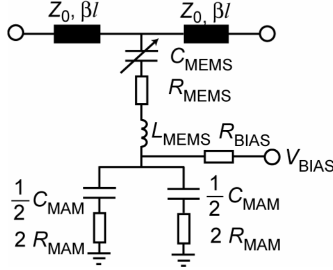

Figure 24. Equivalent circuit for the switched capacitors used in this work [P3–P8].

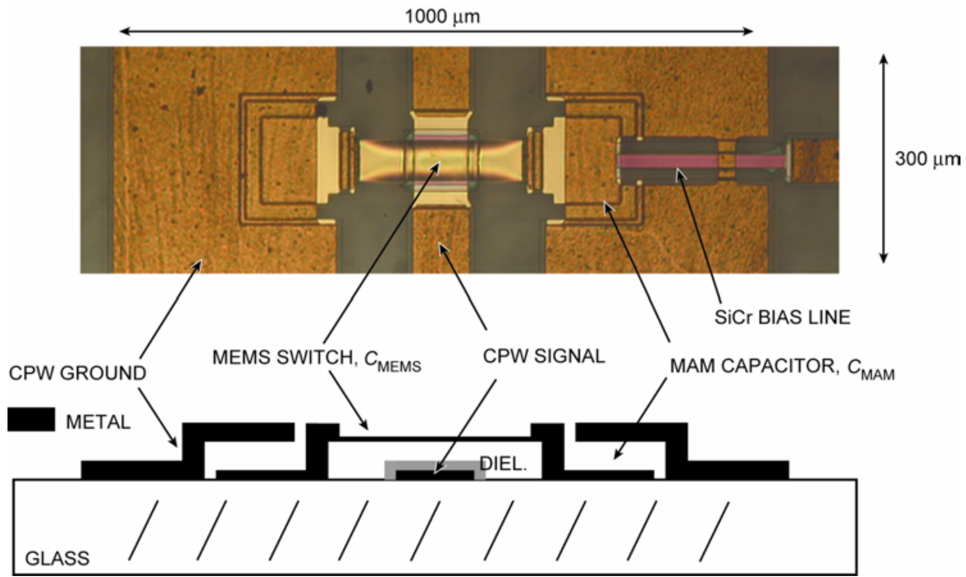

Figure 25. Photograph and cross-sectional view of a switched capacitor used in [P4].

Switched capacitors as in Figure 25 are difficult to use in compact reconfigurable circuits operating above 75 GHz due to their relatively large size. The reason is that the required capacitances and circuit dimensions are quite small at W-band frequencies. Figure 26 presents a novel realization of a W-band switched capacitor developed in this work [P6]. In this case, the anchors are floating and the signal line is connected to the ground using the C_{MEMS} in series with the two C_{MAM}. The anchor area is electroplated to 3–5 µm thickness in order to make it stiff and not flexible.

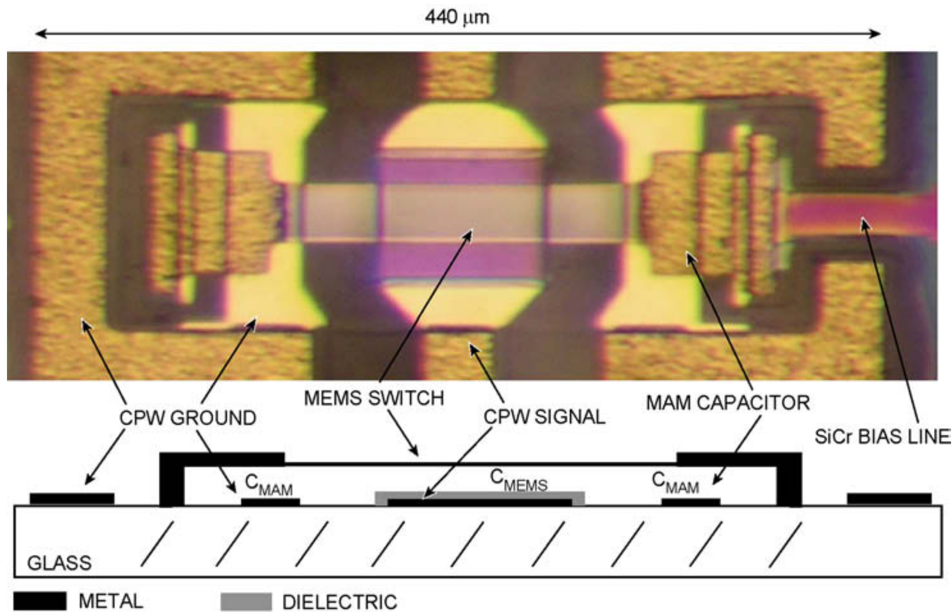

Figure 26. Photograph and schematical cross-sectional view of a W-band switched capacitor developed in this work [P6].

Fabrication process

The fabrication process for switched MEMS capacitors and circuits developed in this work is shown schematically in Figure 27. The process flow is related to Figures 25 and 26, presenting photographs of the fabricated switched capacitors. The fabrication process is a modified six masks version from the surface MEMS process developed before this work at the University of Michigan [103, 104]. The main steps of the process are presented here and detailed process is shown in Appendix A. Corning 7040 glass wafers with $\varepsilon_r = 4.6$ are used as substrates in this work, but the fabrication process is also suitable for other substrates. Only the exposing time of the photoresist in lithography should be adjusted according to the substrate material. High resistivity silicon chrome (SiCr) bias lines are deposited with a sputtering tool and patterned with the lift-off process as the first fabrication step. The second step is the deposition of the bottom electrodes of the MAM capacitors and MEMS switches with an evaporator (Figure 27b). This layer is also patterned with the lift-off process. After that, silicon nitride (Si_xN_y) dielectric layer is deposited with plasma enhanced chemical vapor deposition

(PECVD) followed by reactive ion etch (RIE) patterning (Figure 27c). Polymethylmethacrylate (PMMA) is used as a sacrificial layer under the switches and MAM capacitors, and is patterned using oxygen plasma in the RIE (Figure 27d). A sputtered titanium/gold/titanium (Ti/Au/Ti) layer is used both as the structural layer and seed layer for gold electroplating, which is done after sputtering (Figure 27e). As a final step, MEMS switches are formed with Ti/Au/Ti etching and the sacrificial layer is removed in acetone followed by critical point drying (Figure 27f).

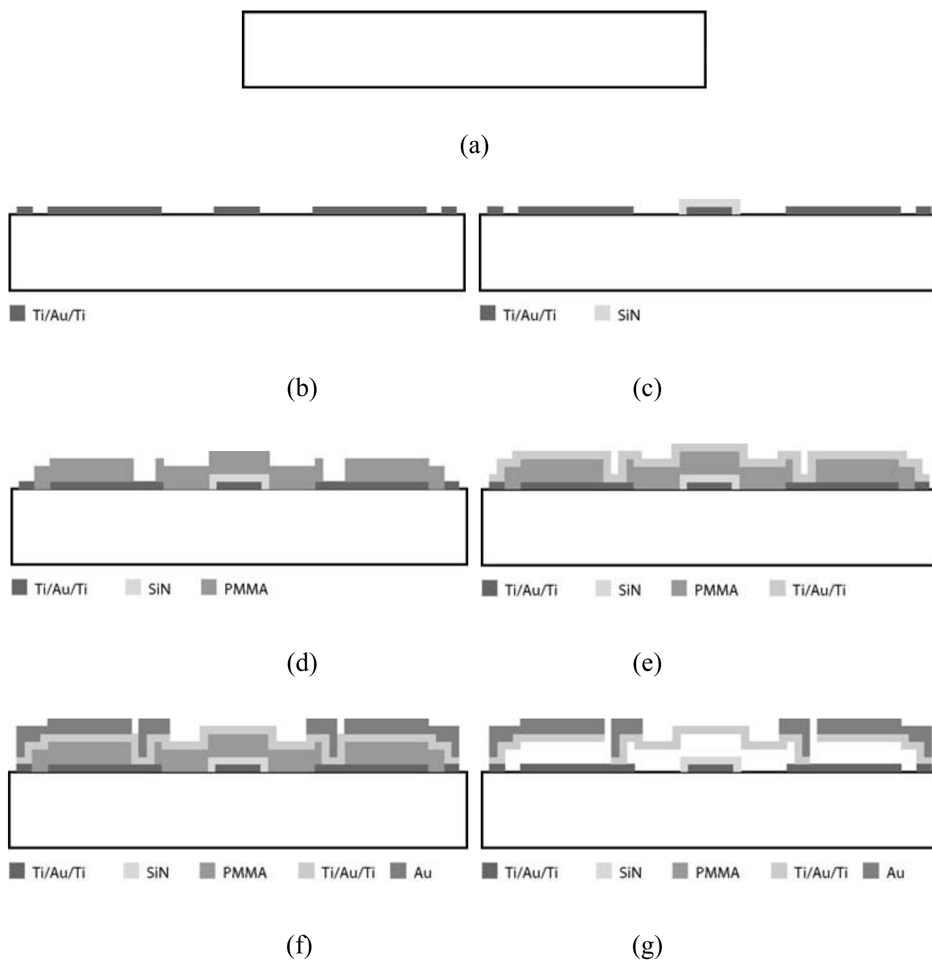

Figure 27. Surface MEMS fabrication process used in this work. The detailed fabrication process is described in Appendix A.

3.2.3 Sliding planar backshorts

In addition to MEMS switches, MEMS technology can be used for other tuning elements. Lubecke et al. realized sliding planar backshorts (SPB) with MEMS technology [35, 105, 106]. The schematical illustration of the SPB in coplanar stripline (CPS) configuration is shown in Figure 28. The metal transmission lines are covered with a dielectric layer and the sliding metal element is on top of these. The sliding element result in a short circuit along the transmission line (capacitively). If the element can be moved, then the position of the short circuit can be changed. Lubecke's sliding planar backshorts were not electrically controllable, and needles were used in on-wafer measurements for changing the place of the SPB on transmission line. However, Lubecke et al. demonstrated successfully that surface micromachining technology is beneficial for millimeter wave applications. Chiao et al. further developed sliding planar backshorts. They used scratch drive actuators (SDA) for the electrical position control of sliding planar backshorts [107, 108].

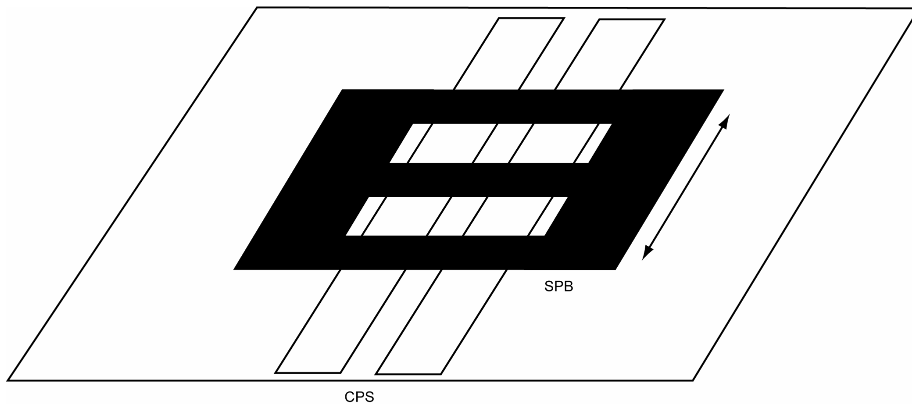

Figure 28. Schematical illustration of a sliding planar backshort (SPB) on CPS configuration.

3.3 Realized impedance tuners

3.3.1 Active device based impedance tuners and matching networks

Bishoff presented the first electronically controllable impedance tuners for measurement purposes [109]. However, the VSWR of the tuner was limited to 6 at 27 GHz. McIntosh et al. showed MMIC designs with improved performance having VSWR of 12.3 and better Smith chart coverage [110]. The simplest impedance tuners or matching networks can be realized with LC networks in T- of π-type configuration [87]. These are suitable to be used as matching networks with power amplifiers or antennas. Matching networks based on *pin* diodes have been realized for applications below 0.4 GHz showing improved matching capability [111]. However, the impedance coverage and $|\Gamma_{MAX}|$ of the impedance tuners and matching network are quite limited due to the resistance of the diodes, varactors, and transistor in all of these active device based impedance tuners.

3.3.2 Impedance tuners based on sliding planar backshorts

The first impedance tuner based on micromachining techniques was published by Lubecke et al. in 1993 for 100 GHz [35], and extended it to 600 GHz later on [106]. These tuners were based on sliding planar backshorts. As described in Section 3.2.3, these were controlled with needles and Chiao et al. developed electrical control for these. They used the tuners for a Vee antenna matching and impedance generation [107, 108]. Measurement results for the antenna were presented demonstrating reconfigurability, but no results for the impedance tuner itself were shown.

3.3.3 Stub-based impedance tuners and matching networks realized with MEMS switches

Kim et al. developed the first impedance tuners based on MEMS switches and varactors, and using the double-stub topology [112]. These tuners were realized with integrated circuit technologies and neither flip-chip nor wire bonding were

in the tuner realizations. Both analog and digital type impedance tuners were presented. The schematics of the tuners are shown in Figure 29. The analog tuner consists of two MEMS varactors, one in each stub. The capacitance of the varactors can be tuned 30 % from their initial value. This method results on fixed frequency impedance tuning at 29 GHz covering two quadrants of the Smith chart. The tuner was targeted for transistor noise matching applications. The digital tuner was realized with 12 MEMS switches having 10.9:1 capacitance ratio, and each switch was controlled separately. The tuner was optimized for optimum load matching of power transistors. The measured results for the tuner showed good impedance coverage for power transistor matching purposes at 29–32 GHz. However, only one quadrant of the Smith chart can be covered. Bandwidths of the tuners developed by Kim et al. were quite narrow (maximum 29–32 GHz), which was the drawback of using short-circuiting switches or low tuning-range analog varactors. The biggest advantage of these tuners compared to MMIC impedance tuners is that they can provide high reflection coefficients. Presented measurement results showed that the digital tuner produces maximum VSWR of 32.3, which is much better than obtained with MMIC impedance tuners.

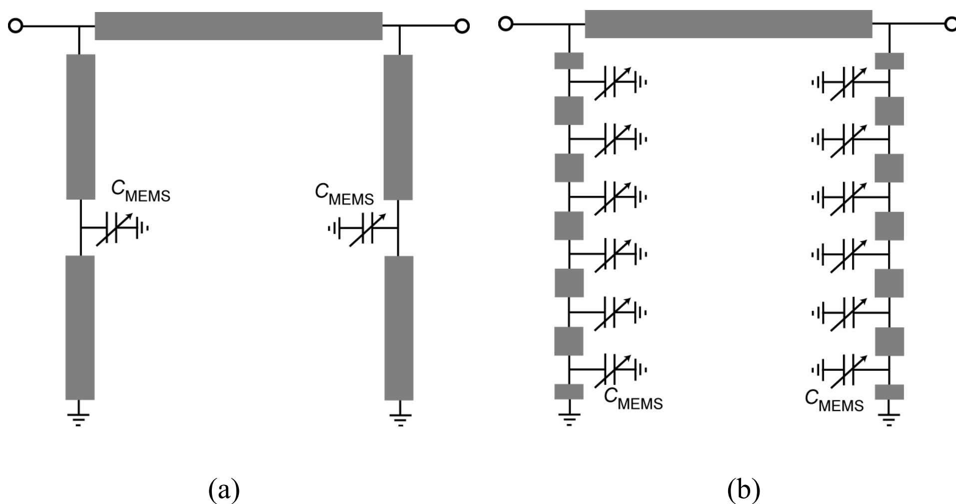

Figure 29. a) Analog and b) digital double-stub impedance tuners realized with MEMS varactors and switches [112].

Papapolymerou et al. [113] presented 2 bit × 2 bit, 3 bit × 3 bit, and 4 bit × 4 bit double-stub tuners. The electrical lengths of the stubs were changed with capacitor banks in the ends of the stubs. They realized capacitor banks with capacitive MEMS switches and fixed capacitors (open-ended microstrip stubs) in series with the switches. Microstrip transmission lines were fabricated on an alumina substrate and MEMS switches with fixed capacitors were wire bonded to the end of the stubs. In addition, biasing networks for the MEMS switches were wire-bonded. The 2 bit × 2 bit tuner provides 16 (2^4) different impedances, 3 bit x 3 bit 64 (2^6), and 4 bit x 4 bit 256 (2^8). The schematic of the 4 bit × 4 bit double-stub impedance tuner is shown in Figure 30. The distance between the stubs is λ/10 at 20 GHz.

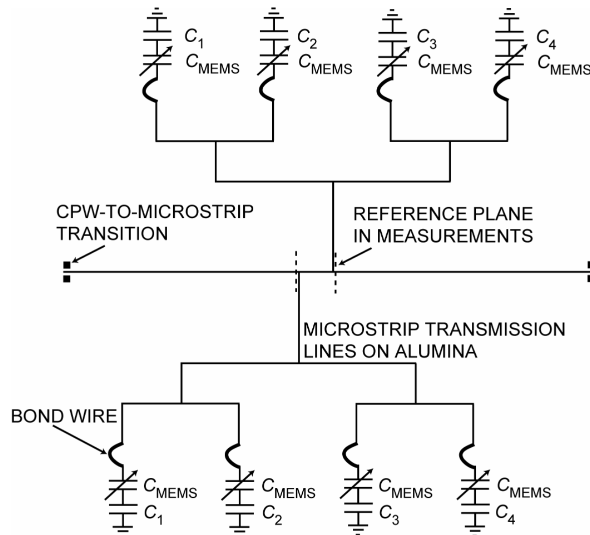

Figure 30. Schematics of the 4 bit × 4 bit double-stub impedance tuner [113].

The 4 bit × 4 bit double-stub impedance tuner had 8 switched capacitor providing 256 different impedances. However, 142 different combinations were measured because of stiction problems of the MEMS switches. Reference planes were transformed to the intersection points of the two stubs. The impedance tuner had moderate impedance coverage at 20 GHz (design frequency) but lower performance was achieved at other frequencies. From two to three quadrants of the Smith chart could be covered with the tuner depending on frequency. The tuner also provided very high reflection coefficients (VSWR = 99), which were possible because both the microstrip lines on alumina and MEMS switches had

very low loss. It should be also noted that the reference planes were transformed mathematically next to the stubs avoiding the loss coming from the CPW to microstrip transitions, input and output transmission line sections, and contact resistance from a probe tip to the contact pads. However, these results were better than results showed for other integrated impedance tuners at the time they were published. Simulations and measurement results also showed a drawback of this realization. Modeling of the tuner was rather difficult because the bond wires were needed to connect the switched capacitors to the stubs. The 4 bit × 4 bit impedance tuner consists of ten chips (transmission lines on alumina, 8 switched capacitor chips, 2 bias network chips) which all should be connected with bond wires. The circuit could be further improved by integrating all parts on the same chip.

A reconfigurable power amplifier was presented by Lu et al. [114]. Reconfigurable input and output matching networks were connected to an RF power transistor in order to use the transistor in 6 and 8 GHz frequency bands. The double-stub tuner topology was used in the matching networks in their work (Figure 31). In this case, the stubs were realized with fixed MIM capacitors and MEMS switches parallel with them. Transmission lines were used only in the section between stubs. The matching networks were designed to be used only with this certain power transistor and need to be redesigned if used with other components. The advantage is that the number of MEMS switches can be minimized as well as the size of the circuit. Lu et al. presented the first results, where a matching network was connected to a power transistor. Also, power amplifier band switching was demonstrated in their work. The amplifier with the reconfigurable input and output matching networks demonstrated 7.2 dB gain with 26.4 % power added efficiency at 6 GHz and 6.1 dB gain with 16.7 % power added efficiency at 8 GHz when the input power was 8 dBm.

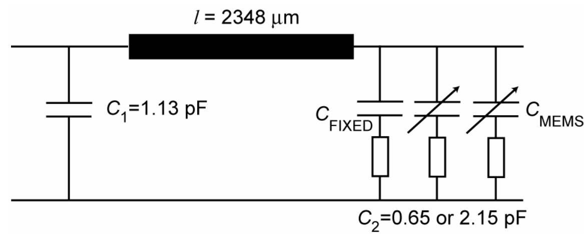

(a)

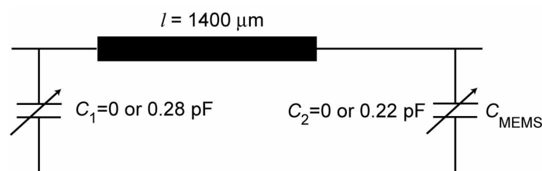

(b)

Figure 31. a) Reconfigurable double-stub input and b) output matching network used for power amplifier band switching [114].

Qiao et al. [115] also published an 8–12 GHz reconfigurable power amplifier with an RF MEMS output impedance tuner based on the double-stub topology. Figure 32 shows the schematics of the 4-bit double-stub output matching network with the varactor (C_{MEMS}), four MEMS switches (C_{MEMS1}–C_{MEMS4}), and eight fixed capacitors (C_1–C_8). The matching network is more advanced version from the double-stub tuners presented Lu et al. in [114]. The varactor can be used for fine tuning of generated impedances. The simulated impedance coverage of the output matching network was presented at 9.6 GHz covering the second quadrant of the Smith chart, which is the optimum load impedance area for the power amplifier. No measurement results for the matching network itself was presented, but the power amplifier reconfigurabality was demonstrated over 7–11 GHz frequency band.

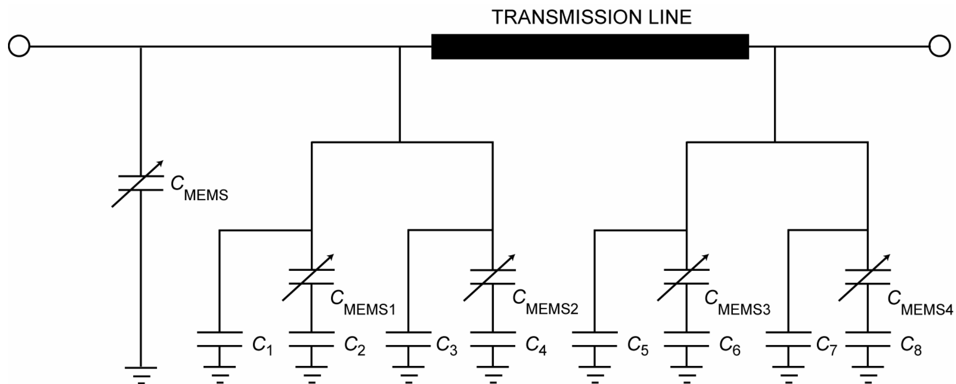

Figure 32. Schematics of a double-stub matching network developed by Qiao et al. [115].

MEMS varactors were developed at Nokia by Nieminen et al. [116, 117]. A simple 1-bit LC-matching network was demonstrated for 880–915 MHz cellular phone applications by combining a high-Q inductor and MEMS capacitor [118]. The power consumption of a power amplifier was lowered by 42 % at 23 dBm power level with the matching network. This matching network is the only published packaged RF MEMS matching network circuit. The drawbacks of the matching network are that it has to be redesigned for different amplifiers and it is quite sensitive for parasitics like bond wires. The main reason for this is that only one bit can be used. However, only one switch is needed reducing the cost, control logic, and size, which are very important factors in cellular phone applications.

In all stub-based tuners described here [112–115], the electrical length and/or impedance of stubs are changed but the electrical distance between the stubs is fixed. This limits both the impedance coverage and bandwidth of the impedance tuners and matching networks. Switched capacitors were applied to stub topologies in this work [P3–P6]. A single switched capacitor has mainly two effects between its two states: the delay and impedance of a transmission line can be changed. Figure 33 shows the schematics of the single, double, and triple-stub topologies with switched capacitors. In this work, the switched capacitors are distributed along to the stubs and also to the sections between the stubs. Because the switched capacitors are distributed along the stubs, more impedances can be generated compared to the situation where the switched capacitors are just at the end of the stubs. Figure 34 shows the fabricated triple-stub tuners that have been developed for 6–24 GHz and 75–115 GHz.

In this work, the stub-based impedance tuners were optimized for noise parameter measurement applications. Publication [P3] presents triple-stub tuners with 11 and 13 switched capacitors, a double-stub tuner with 11 switched capacitors, and a single-stub impedance tuner with 10 switched capacitors. All of the tuners are for 6–24 GHz, and have better and more wideband impedance coverage than any other published integrated impedance tuner in this frequency range. Also, the measured maximum available reflection coefficient $|\Gamma_{MAX}|$ is comparable to other published integrated impedance tuners being 0.99 (equal to VSWR of 199) at 30 GHz for the double-stub tuner. Comparison of published integrated impedance tuners for frequencies below 30 GHz is shown in Table 1 also shows the advantage of using MEMS technology in integrated impedance tuners because they can produce very high reflection coefficients.

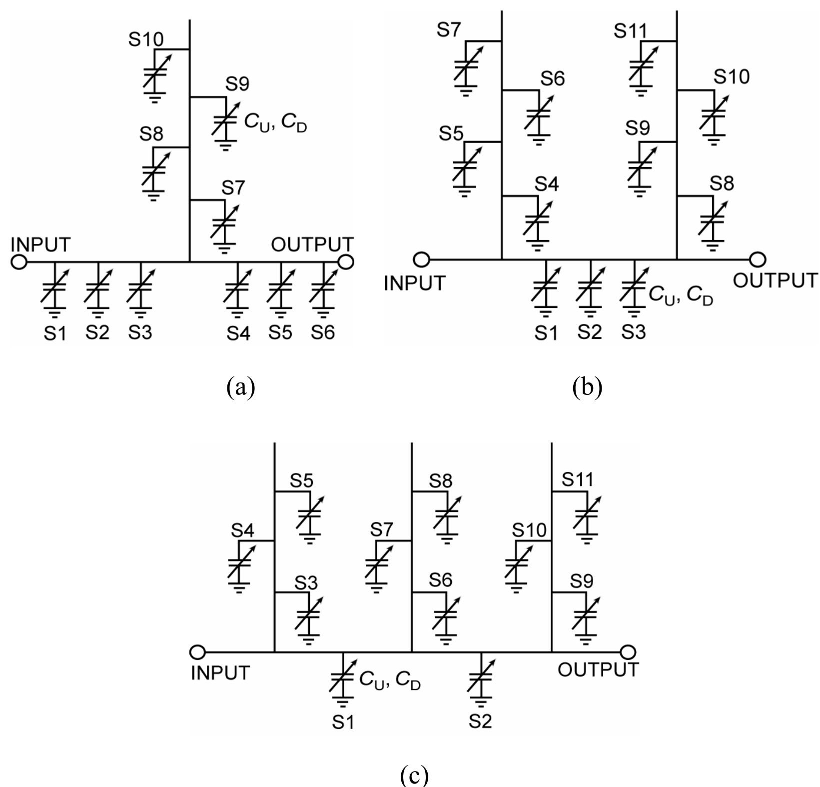

Figure 33. Schematics of the stub-based impedance tuners where the impedance tuning is realized with switched capacitors (S1–S11). a) The single-stub tuner, b) double-stub tuner, and c) triple-stub tuner [P3–P6]. Notice that both the stubs and the transmission line between the stubs (or before and after as in (a)) are tuned.

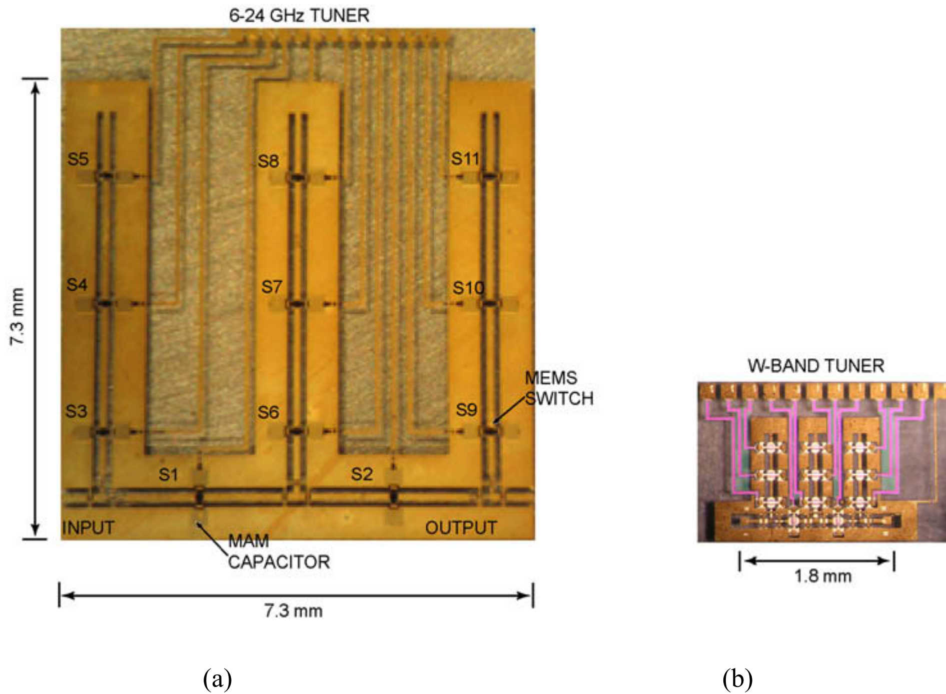

(a) (b)

Figure 34. a) Photograph of the fabricated 6–24 GHz 3-stub impedance tuner [P3] and b) W-band 3-stub impedance tuner [P6].

The single-stub tuner was extended to 20–50 GHz, and a V-band design (50–80 GHz) was also realized with 10 switched MEMS capacitors [P4, P5]. Both tuners can generate 1024 (2^{10}) different impedances. The 20–50 GHz single-stub impedance tuner has more wideband operation than other integrated tuners operating at the lower part of the frequency band [112, 113]. Measured $|\Gamma_{MAX}|$ is 0.86, 0.88, 0.94 at 20, 30, and 40 GHz from 160 measurement points out of 1024 possible combinations for the 20–50 GHz impedance tuner. The results for the V-band single-stub impedance tuner are unique being the only published results for integrated impedance tuners at this frequency range [P5]. Measured $|\Gamma_{MAX}|$ is 0.90 at 60 GHz and 0.99 at 78 GHz (equal to VSWR of 199) from 90 measurements out of 1024 possible combinations. Also, the results for W-band double and triple-stub impedance tuners presented in [P6] are the only published results for integrated impedance tuners at W-band.

Table 1. VSWR comparison of published integrated impedance tuners for frequencies 5–30 GHz.

Reference	Technology	VSWR	Freq. (GHz)
[109]	HEMT	6	27
[110]	HEMT	12.3	18
[112]	MEMS	32.3	30
[113]	MEMS	99	20
[P3]	MEMS	199	30

3.3.4 Distributed impedance tuners and matching networks realized with MEMS switches

The phase velocity and impedance of a transmission line can be changed by loading it capacitively. This idea has been used successfully in distributed MEMS transmission-line (DMTL) phase-shifters [25] and filters [119]. Distributed type phase shifters can be easily modified to be used as tunable quarter-wave impedance transformers. Both the electrical length and impedance of the transmission line can be changed and controlled very accurately [25, 27, 30, 100–102]. Because the impedance and electrical length of the transmission line are changed in a distributed manner, low loss and high power handling capability can be achieved.

Distributed type matching networks were developed for amplifier and antenna matching applications as well as for noise parameter and load-pull measurement applications in this work [P7–P8]. A transmission line is loaded with switched capacitors in this approach (Figure 35). Each switched capacitor has two states having two different capacitances, namely C_1 and C_2. In this work, the switched capacitors were realized with MEMS switches (C_{MEMS}) in series with fixed metal-air-metal capacitors (C_{MAM}). The capacitance of the MEMS switches was matched with a high impedance transmission line so that the impedance of the loaded transmission line was close to 50-Ω in the up-state position of the MEMS switches. The high impedance unloaded transmission line at microwave

frequencies is effectively the same as an inductor-based matching at lower frequencies. By switching down more and more MEMS switches, the loading capacitance increases, transmission line impedance decreases, and the electrical length of the transmission line increases. Both 4 and 8-switch versions of distributed reconfigurable matching networks were realized for 4–18 GHz and an 8-switch version for 20–50 GHz amplifiers.

Publication [P7] describes the development of a novel reconfigurable matching network based on the loaded-line technique. The network is composed of N-switched capacitors (N = 4...8) with a capacitance ratio of 4:1 to 5:1, and is suitable for power amplifiers at 4–18 GHz, or as an impedance tuner for noise parameter and load-pull measurements at 10–28 GHz. The networks are very small, and offer better performance than double or triple stub matching networks. Extensive loss analysis indicates that the 8-element network has a loss of 0.5 dB at 4–12 GHz, and less than 1.5 dB at 18 GHz, even when matching a 10 Ω output impedance to a 50 Ω load. As expected, the 4-element matching network has about half the loss of the 8-element network but with much less impedance coverage. Both networks were simulated and measured in high VSWR conditions and can handle at least 500 mW of RF power at 4–18 GHz. The application areas are in phased array antennas and reconfigurable power amplifiers.

Publication [P8] presents extension of the distributed reconfigurable matching networks to 20–50 GHz power amplifier applications (see Figure 35). The matching network consists of 8 switched MEMS capacitors producing 256 (2^8) different impedances and is only 1×2.5 mm^2 in size on a glass substrate. The network is ideally suited to match power amplifiers with 10–20 Ω output impedance to 50–60 Ω systems at 20–50 GHz. The estimated loss of the network is only 1–1.5 dB at 40 GHz while matching a 10–20 Ω load to a 50 Ω load. The reconfigurable network can also be used as an impedance tuner in noise parameter and load-pull measurements of active devices at 30–65 GHz.

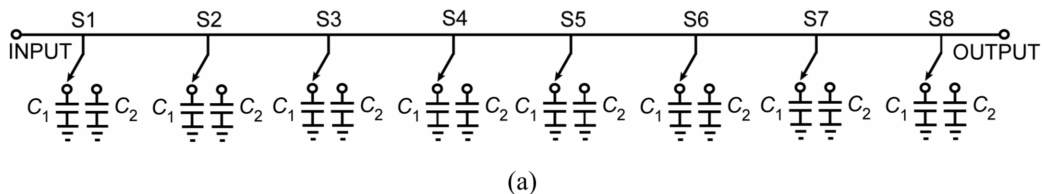

(a)

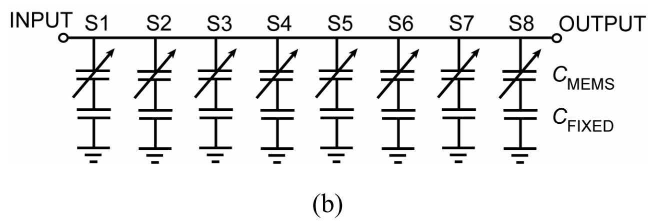

(b)

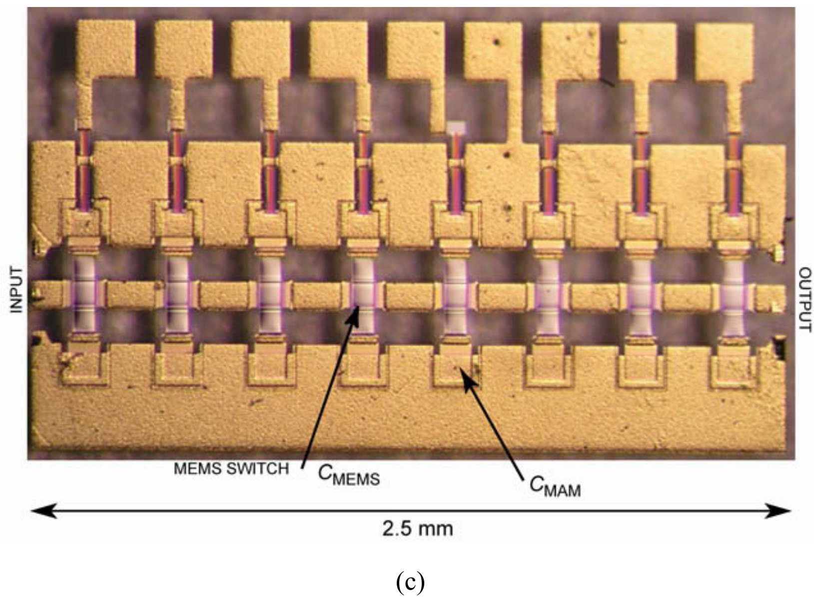

(c)

Figure 35. a) Schematics of a transmission line loaded with switched capacitors and b) switched capacitors realized with MEMS switches in series with switched capacitors. c) Photograph of a fabricated 20–50 GHz reconfigurable matching network [P8].

Shen and Barker have presented a distributed type impedance tuner based on the double-slug topology [120]. The schematic of a double-slug impedance tuner is shown in Figure 36. It has two 90° low impedance sections, the length of which determines the center frequency of the tuner, and the lengths L_1 and L_2 define the

impedance point being matched. Shen and Barker realized the double-slug tuner based on a DMTL, and having an individual bias control in each MEMS switched capacitor (totally 80 MEMS switched capacitors). The maximum VSWR generated by the tuner is VSWR = $(Z_0/Z_L)^4$, and was 4 in this case. This realization allows low loss and wideband operation with good impedance coverage inside the VSWR circle limited by $(Z_0/Z_L)^4$. The drawbacks of this realization are large number of control signals (80 in this case) and quite low maximum VSWR.

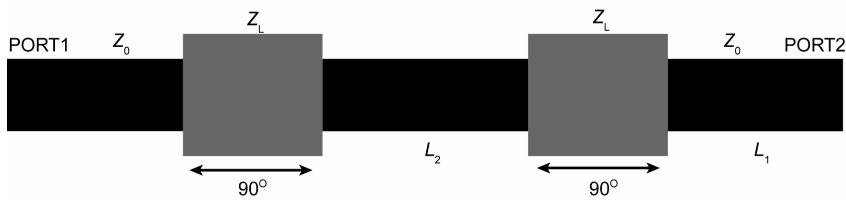

Figure 36. Schematic of the double-slug tuner [120].

4. Summary of publications

Publication [P1] presents an on-wafer noise parameter measurement set-up for W-band device characterization. Detailed description of the developed measurement system and procedures has been given. The noise parameters of an InP HEMT (DaimlerChrysler 2 × 40 μm) have been measured, and measurement results have been presented in the 79–94 GHz frequency band. These are the first and only published on-wafer noise parameter measurement results for an active device above 75 GHz.

Publication [P2] presents on-wafer measurement system for wideband cryogenic device characterization. A V-band waveguide based measurement system has been extended to W-band. The S-parameters of HEMTs (DaimlerChrysler and HRL) has been measured at W-band and also in the 50–110 GHz frequency band and at 20–295 K. These are the first and only published cryogenic measurement results at this frequency range.

Publication [P3] introduces integrated triple, double, and single-stub impedance tuners for 6–24 GHz applications. Novel method for impedance tuning based on switched MEMS capacitors has been used in the tuners. The tuners have 10–13 switched capacitors producing 1024–8192 (2^{10}–2^{13}) different impedances. The impedance coverage of the tuners is the widest measured to-date from any integrated tuner at this frequency range. Also, the tuners can produce high reflection coefficients. The maximum measured $|\Gamma_{MAX}|$ has been 0.99 (equal to VSWR 199) for the double-stub tuner at 30 GHz.

Publication [P4] describes the design, fabrication, and measurement results for a 20–50 GHz single-stub RF MEMS impedance tuner. The design is based on combining the loaded line technique with the single-stub topology to obtain wide impedance coverage with high $|\Gamma_{MAX}|$. The tuner consists of ten switched MEMS capacitors producing 1024 (2^{10}) different impedances. The design has been optimized for noise parameter and load-pull measurements of active devices and shows excellent measured impedance coverage over the 20–50 GHz frequency range. Measured $|\Gamma_{MAX}|$ is 0.86, 0.88, 0.94 at 20, 30, and 40 GHz from 160 measurements out of 1024 possible combinations, respectively.

Publication [P5] presents a single-stub RF MEMS impedance tuner optimized for 50–80 GHz noise parameter and load-pull measurement applications. This is the first and only published integrated impedance tuner operating at V-band (50–75 GHz). The tuner is small enough to be integrated inside an RF measurement probe. Measured (90 measurements out of 1024 possible combinations) $|\Gamma_{MAX}|$ is 0.81, 080, 0.90, 0.94, 0.97, 0.99, and 0.99 at 50, 55, 60, 65, 70, 75, and 78 GHz, respectively. The tuner can be used as a reflection type impedance tuner over 40–80 GHz frequency band, when the output of the tuner is terminated with an open circuit.

Publication [P6] shows reconfigurable integrated double and triple-stub impedance tuners operating at W-band. The impedance tuners are based on 11 switched MEMS capacitors producing 2048 (2^{11}) different impedances. Also, novel realization for switched capacitors is presented allowing compact size and accurate capacitance control. Measured $|\Gamma_{MAX}|$ is 0.93, 0.87 and 0.87 at 75, 90, and 105 GHz for the double-stub tuner from 110 measurements and 0.92, 0.87, and 0.83 for the triple-stub tuner from 90 measurements out 2048 combinations.

Publication [P7] describes the development of a novel reconfigurable matching network based on the loaded-line technique. The network is composed of N-switched capacitors (N = 4...8) with a capacitance ratio of 4:1 to 5:1 and is suitable for power amplifiers at 4–18 GHz, or as an impedance tuner for noise parameter and load-pull measurements at 10–28 GHz. The networks are very small, and offer better performance than double or triple stub matching networks. Extensive loss analysis indicates that the 8-element network has a loss of 0.5 dB at 4–12 GHz, and less than 1.5 dB at 18 GHz, even when matching a 10 Ω output impedance to a 50-Ω load. As expected, the 4-element matching network has about half the loss of the 8-element network but with much less impedance coverage. Both networks were simulated and measured in high VSWR conditions and can handle at least 500 mW of RF power at 4–18 GHz. The application areas are in phased array antennas, reconfigurable power amplifiers, and wideband noise parameter and load-pull measurement systems.

Publication [P8] presents extension of the distributed reconfigurable matching networks to 20–50 GHz power amplifier applications. The matching network consists of 8 switched MEMS capacitors producing 256 (2^8) different impedances and is only 1 × 2.5 mm in size on a glass substrate. The network is

ideally suited to match power amplifiers with 10–20 Ω output impedance to 50–60 Ω systems at 20–50 GHz. The estimated loss of the network is only 1–1.5 dB at 40 GHz while matching a 10–20 Ω load to a 50-Ω load. The reconfigurable network can also be used as an impedance tuner in noise parameter and load-pull measurements of active devices at 30–65 GHz.

5. Conclusion

This thesis extended both on-wafer cryogenic and noise parameter measurements to W-band frequencies. For the first time, noise parameters of an active device were measured at W-band. Also, wideband cryogenic on-wafer measurements have been carried out for transistors between 50 and 110 GHz and 20–295 K.

In order to further develop on-wafer noise parameter measurement methods, novel RF MEMS impedance tuners were designed, fabricated, and characterized in this thesis work. The integrated tuners were based on single, double, and triple-stub topologies and CPW transmission lines on glass substrate. The electrical tuning of the electrical length and transmission line impedance were realized innovatively with switched MEMS capacitors. By using N (number of switched capacitors) switched capacitors, 2^N different impedances could be generated. The stub-based impedance tuners were realized with 10, 11, or 13 switched capacitors producing 1024, 2048, or 8192 different impedances. Several tuners were developed to cover 6–120 GHz frequency band. Single, double, and triple-stub tuners were developed for the 6–24 GHz band, a single-stub tuner for 20–50 GHz, a single stub tuner for 40–80 GHz, and both double and triple-stub tuners for 75–120 GHz. The highest reflection coefficients were measured from the 6–30 GHz double-stub tuner at 30 GHz and from the 40–80 GHz single-stub impedance tuner at 78 GHz having $|\Gamma_{MAX}|$ of 0.99 which is equal to VSWR 199. The developed stub-based impedance tuners have the state-of-the-art performance compared to any other published integrated impedance tuners having the widest impedance and frequency coverage with highest measured $|\Gamma_{MAX}|$.

In addition to the stub-based impedance tuners, novel distributed reconfigurable matching networks were developed for 4–18 GHz and 20–50 GHz applications. The switched capacitor tuning was also applied to the distributed topology. These matching networks are most suitable for multi-band and reconfigurable applications, where systems need to operate at several frequencies over a wide frequency range and must tolerate changing impedance conditions. The distributed matching networks have lower loss and better RF power handling capabilities compared to the stub-tuners.

Future work includes further development of on-wafer measurement methods and especially characterization of RF MEMS components and circuits. Also, research will focus to the improvement of reconfigurable matching networks and impedance tuners, realization of RF MEMS circuits above 140 GHz, investigation of CMOS compatible fabrication methods for MEMS components and circuits for millimeter wave applications, and development of electrically steerable antenna arrays based on MEMS technology.

References

1. T. Vähä-Heikkilä, J. Varis, H. Hakojärvi, and J. Tuovinen, "Cryogenic on-wafer measurements at W-band and at 20–295 K." *The 3rd ESA Workshop Millimetre Wave Technology and Applications: Antennas, Circuits, and Systems*, Espoo, Finland, 2003. Pp. 435–439.

2. T. Vähä-Heikkilä, M. Lahdes, M. Kantanen, T. Karttaavi, and J. Tuovinen, "Very wideband automated on-wafer noise figure and gain measurements at 50–110 GHz." *Proceedings of GAAS 2002, The European Gallium Arsenide & related III–V Compounds Applications Symposium*, Milan, Italy, 2002. Pp. 233–236.

3. T. Vähä-Heikkilä, M. Kantanen, M. Lahdes, and J. Tuovinen, "Practical methods for millimeter wave on-wafer measurements of active devices at 50–110 GHz." *Proceedings of the International Joint Conference of the Sixth Topical Symposium on Millimeter Waves (TSMMW2004) and the Fifth MINT Millimeter-Wave International Symposium (MINT-MIS)*, Yokosuka, Japan, 2004. Pp. 118–121.

4. M. Kantanen, M. Lahdes, T. Vähä-Heikkilä, J. Tuovinen, "A wideband automated measurement system for on-wafer noise parameter measurements at 50–75 GHz." *IEEE Transactions on Microwave Theory and Techniques,* Vol. 51, No. 5, pp. 1489–1495, 2003.

5. T. Vähä-Heikkilä, "*Wideband Cryogenic and Room Temperature On-Wafer Measurements at 50–110 GHz.*" Licentiate thesis, University of Turku, 2005.

6. T. Vähä-Heikkilä, J. Varis, J. Tuovinen, G.M. Rebeiz, "Reconfigurable RF MEMS impedance tuners and matching networks." *The 34th European Microwave Conference, Proceedings of Workshop on Smart MEMS for RF and Millimeter Wave Communications,* Amsterdam, Netherlands, 2004. Pp. 123–136.

7. M.W. Pospieszalski, E.J. Wollack, N. Bailey, D. Thacker, J. Webber, L.D. Nguyen, N. Le, and M. Lui, "Design and performance of wideband, low-noise, millimeter-wave amplifiers for Microwave Anisotropy Probe radiometers." *2000 IEEE MTT-S International Microwave Symposium Digest*, Boston, MA, 2000. Pp. 25–28.

8. J. Tuovinen, P. Kangaslahti, P. Haapanen, N. Hughes, P. Jukkala, T. Karttaavi, O. Koistinen, M. Lahdes, H. Salminen, and J. Tanskanen, S. Urpo, "Development of 70 GHz receivers for the Planck LFI." *Astrophysics Letters and Communications*, Vol. 37, pp. 181–187, 2000.

9. P. J. Napier, D. S. Bagri, B.G. Clark, A.E.E. Rogers, J.D. Romney, A.R. Thompson, and R.C. Walker, "The Very Long Baseline Array." *Proceedings of the IEEE*, Vol. 82, No. 5, pp. 656–672, 1994.

10. A. Wootten, ed., *Science with the Atacama Large Millimeter Array*, San Francisco, CA, ASP, Vol. 253, 2001.

11. L.H. Eriksson and B. As, "A high performance automotive radar for automatic AICC." *IEEE Aerospace and Electronic Systems Magazine*, Vol. 10, No. 12, pp. 13–18, 1995.

12. H. Meinel, J. Wenger, H. Hentling, G. Rollmann, and H. Dominik, "Automotive radar: from long range collision warning to short range urban employment." *Proceedings of the International Joint Conference of the Seventh Topical Symposium on Millimeter Waves (TSMMW2004) and the Sixth MINT Millimeter-Wave International Symposium (MINT-MIS)*, Seoul, Korea, 2005. Pp. 244–247.

13. P. Mikkonen, "Modern 60 GHz radio link." *Proceedings of the 29th European Microwave Conference*, Munich, Germany, Vol. 3, 1999. Pp. 83–86.

14. M. Kärkkäinen, M. Varonen, J. Riska, P. Kangaslahti, and V. Porra, "A set of integrated circuits for 60 GHz radio front-end." *2002 IEEE MTT-S International Microwave Symposium Digest,* Seattle, WA, Vol. 2, 2002. Pp. 1273–1276.

15. M. Varonen, M. Kärkkainen, P. Kangaslahti, and V. Porra, "Integrated power amplifier for 60 GHz wireless applications." *2003 IEEE MTT-S International Microwave Symposium Digest*, Philadelphia, PA, Vol. 2, 2003. Pp. 915–918.

16. K. Hmaguchi, Y. Shoji, H. Ogawa, Y.H. Kim, and S. Shimizu, "Millimeter-wave vertically connected wireless link system – system overview." *Proceedings of the International Joint Conference of the Seventh Topical Symposium on Millimeter Waves (TSMMW2004) and the Sixth MINT Millimeter-Wave International Symposium (MINT-MIS)*, Seoul, Korea, 2005. Pp. 255–258.

17. L. Yujiri, M. Shoucri, and P. Moffa, "Passive millimeter wave imaging." *IEEE Microwave Magazine*, Vol. 4, No. 3, pp. 39–50, 2003.

18. R.M. Smith, K.D. Trott, B.M. Sundstrom, and D. Ewen, "The passive mm-wave scenario." *Microwave Journal*, Vol. 39, No. 3, pp. 22–34, 1996.

19. M. Kantanen, M. Lahdes, and J. Tuovinen, "A millimeter wave imager." *Proceedings of the International Joint Conference of the Seventh Topical Symposium on Millimeter Waves (TSMMW2004) and the Sixth MINT Millimeter-Wave International Symposium (MINT-MIS)*, Seoul, Korea, 2005. Pp. 240–243.

20. J. Rizk, G.-L. Tang, J.B. Muldavin, and G.M. Rebeiz, "High-isolation W-band MEMS switches." *IEEE Microwave and Wireless Components Letters*, Vol. 11, No. 1, pp. 10–12, 2001.

21. J. Rizk and G.M. Rebeiz, "W-band microstrip RF-MEMS switches and phase shifters." *2003 IEEE MTT-S International Microwave Symposium Digest*, Philadelphia, PA, 2003. Pp. 1485–1488.

22. J. Rizk and G.M. Rebeiz, "W-band CPW RF MEMS circuits on quartz substrates." *IEEE Transactions on Microwave Theory and Techniques*, Vol. 51, No. 7, pp. 1857–1862, 2003.

23. D. Mercier, P.L. Charvet, P. Berruyer, C. Zanchi, L. Lapierre, O. Vendier, J.L. Cazaux, and P. Blondy, "A DC to 100 GHz high performance ohmic shunt switch." *2004 IEEE MTT-S International Microwave Symposium Digest*, Fort Worth, TX, 2004. Pp. 1931–1934.

24. J. Schobel, T. Buck, M. Reimann, M. Ulm, and M. Schneider, "W-band RF-MEMS subsystems for smart antennas in automotive radar sensors." *Proceedings of the 34th European Microwave Conference 2004*, Amsterdam, Netherlands, 2004. Pp. 1305–1308.

25. N.S. Barker and G.M. Rebeiz, "Optimization of distributed MEMS transmission line phase shifters – U-band and W-band designs." *IEEE Transactions on Microwave Theory and Techniques*, Vol. 48, No. 11, pp. 1957–1966, 2000.

26. H.-T. Kim, J.-H. Park, J. Yim, Y.-K. Kim, and Y. Kwon, "A compact V-band 2-bit reflection-type MEMS phase shifter." *IEEE Microwave and Wireless Components Letters*, Vol. 12, No. 9, pp. 324–326, 2002.

27. H.-T. Kim, J.-H. Park, S. Lee, S. Kim, J.-M. Kim, Y.-K. Kim, and Y. Kwon, "V-band 2-b and 4-b low-loss and low-voltage distributed MEMS digital phase shifter using metal-air-metal capacitors." *IEEE Transactions on Microwave Theory and Techniques*, Vol. 50, No. 12, pp. 2918–2923, 2002.

28. H.-T. Kim, S. Lee, J.-M. Kim, J.-H. Park, Y.-K. Kim, and Y. Kwon, "A V-band CPS distributed analog MEMS phase shifter." *2003 IEEE MTT-S International Microwave Symposium Digest*, Philadelphia, PA, 2003. Pp. 1481–1484.

29. J.-J. Hung, L. Dussopt, and G.M. Rebeiz, "Distributed 2- and 3-bit W-band MEMS phase shifters on glass substrates." *IEEE Transactions on Microwave Theory and Techniques*, Vol. 52, No. 2, pp. 600–606, 2004.

30. B. Lakshminarayanan and T. Weller, "MEMS phase shifters using cascaded slow-wave structures for improved impedance matching and/or phase shift." *2004 IEEE MTT-S International Microwave Symposium Digest*, Fort Worth, TX, 2004. Pp. 725–728.

31. H.-T. Kim, J.-H. Park, Y.-K. Kim, and Y. Kwon, "Low-loss and compact V-band MEMS-based analog tunable bandpass filters." *IEEE Microwave and Wireless Components Letters*, Vol. 12, No. 11, pp. 432–434, 2002.

32. E. Fourn, C. Quendo, E. Rius, A. Pothier, P. Blondy, C. Champeaux, J.C. Orlianges, A. Catherinot, G. Tanne, C. Person, and F. Huret, "Bandwidth and central frequency control on tunable bandpass filter by using MEMS cantilevers." *2003 IEEE MTT-S International Microwave Symposium Digest*, Philadelphia, PA, 2003. Pp. 523–526.

33. S. Lee, J.-H. Park, J.-M. Kim, H.-T. Kim, Y.-K. Kim, and Y. Kwon, "A compact low-loss reconfigurable monolithic low-pass filter using multiple-contact MEMS switches." *IEEE Microwave and Wireless Components Letters*, Vol. 14, No. 1, pp. 37–39, 2004.

34. B. Schoenlinner, A. Abbaspour-Tamijani, L.C. Kempel, and G.M. Rebeiz, "Switchable low-loss RF MEMS Ka-band frequency-selective surface." *IEEE Transactions on Microwave Theory and Techniques*, Vol. 52, No. 11, pp. 2474–2481, 2004.

35. V.M. Lubecke, W.R. McGrath, and D.B. Rutledge, "A 100-GHz coplanar strip circuit tuned with a sliding planar backshort." *IEEE Microwave Guided Wave Letters,* Vol. 3, No. 12, pp. 441–443, 1993.

36. C.-W. Baek, S. Song, C. Cheon, Y.-K. Kim, and Y. Kwon, "2-D mechanical beam steering antenna fabricated using MEMS technology." *2001 IEEE MTT-S International Microwave Symposium Digest*, Phoenix, AZ, 2001. Pp. 211–214.

37. B. Lakshminarayanan and T. Weller, "Electronically tunable multi-line TRL using an impedance matched multi-Bit MEMS phase shifter." *IEEE Microwave and Wireless Components Letters*, Vol. 15, No. 2, pp. 137–139, 2005.

38. F. Ulaby, R. Moore, and A. Fung, *Microwave Remote Sensing, Active and Passive*, Vol. 1. Addison–Wesley Publishing Company, Reading, MA, 1981.

39. L.A. Klein, *Millimeter-Wave and Infrared Multisensor Design and Signal Processing*, Artec House, Norwood, MA, 1997.

40. E.H. Armstrong, "The super-heterodyne – its origin, development, and some recent improvements." *Proceedings of the IRE*, Vol. 50, pp. 539–552, 1924.

41. A.R. Barnes, P. Munday, R. Jennings, M. Moore, M. Black, R. Appleby, R. Anderton, G. Sinclair, and P Coward, "MMIC Technology and its application in passive mm-wave imaging systems." *The 3rd ESA Workshop Millimetre Wave Technology and Applications: Antennas, Circuits, and Systems*, Espoo, Finland, 2003. Pp. 543–547.

42. J. Tuovinen, N. Hughes, P. Jukkala, P. Kangaslahti, T. Karttaavi, P. Sjöman, and J. Varis, "Technology for millimetre wave radiometers." *Proceedings of the 33rd European Microwave Conference*, Munich, Germany, 2003. Pp. 883–886.

43. S.Y. Liao, *Microwave Circuit Analysis and Amplifier Design*. Prentice–Hall, Englewood Cliffs, NJ, 1987.

44. E.W. Strid and K.R. Gleason: "A DC-12 GHz monolithic GaAsFET distributed amplifier." *IEEE Transactions on Microwave Theory and Techniques*, Vol. 82, No. 7, pp. 969–975, 1982.

45. E.W. Strid and K.R. Gleason, "Calibration methods for microwave wafer probing." *Microwave and Millimeter-Wave Monolithic Circuits*, Vol. 84, No. 1, pp. 78–82, 1984.

46. M. Matloubian, S.E. Rosenbaum, H.R. Fetterman, and P.T. Greiling, "Wide-band millimeter wave characterization of sub-0.2 micrometer gate-length AlInAs/GaInAs HEMTs." *IEEE Microwave and Guided Wave Letters*, Vol. 1, No. 2, pp. 32–34, 1991.

47. R.Y. Yu, J. Pusl, Y. Konishi, M. Case, M. Kamegawa, and M. Rodwell, "8–96 GHz on-wafer network analysis." *Technical Digest of 14th Annual Gallium Arsenide Integrated Circuit (GaAs IC) Symposium 1992*, 1992. Pp. 75–77.

48. R. Anholt, J. Pence, and E. Godshalk, "On-wafer HEMT characterization to 110 GHz." *Technical Digest of the 16th Annual Gallium Arsenide Integrated Circuit (GaAs IC) Symposium 1994*, 1994. Pp. 108–111.

49. R. Lai, M. Barsky, T. Huang, M. Sholley, H. Wang, Y.L. Kok, D.C. Streit, T. Block, and P.H. Liu, "An InP HEMT MMIC LNA with 7.2-dB gain at 190 GHz." *IEEE Microwave and Guided Wave Letters*, Vol. 8, No. 11, pp. 393–395, 1998.

50. C.W. Pobanz, M. Matloubian, M. Lui, H.-C. Sun, M. Case, C.M. Ngo, P. Janke, T. Gaier, and L. Samoska, "A high-gain monolithic D-band InP HEMT amplifier." *IEEE Journal of Solid-State Circuits*, Vol. 34, No. 9, pp. 1219–1224, 1999.

51. A. Tessmann, O. Wohlgemuth, R. Reuter, W. Haydl, H. Massler, and A. Hulsmann, "A coplanar 148 GHz cascode amplifier MMIC using 0.15 μm GaAs PHEMTs." *2000 IEEE MTT-S International Microwave Symposium Digest*, Boston, MA, Vol. 2, 2000. Pp. 991–994.

52. T.-N. Ton, H. Wang, S. Chen, K.L. Tan, G.S. Dow, B.R. Allen, and J. Berenz, "W-band monolithic pseudomorphic AlGaAs/InGaAs/GaAs HEMT CBCPW LNA." *Electronics Letters*, Vol. 29, No. 20, pp. 1804–1805, 1993.

53. T. Katoh, T. Kashiwa, H. Koski, A. Inoue, and T. Ishikawa, "Automated millimeter-wave on-wafer testing system." *IEICE Transaction on Electron.*, Vol. E82-C, pp. 1312–1317, 1999.

54. M.G. Case, C. Pobanz, S. Weinreb, M. Matloubian, M. Hu, M. Wetzel, P. Janke, and C. Ngo, "Low-cost, high-performance W-band LNA MMICs for millimeter-wave imaging." *Proceedings of Spie, Passive Millimeter-Wave Imaging Technology IV*, Vol. 4032, pp. 89–96, 2000.

55. A. Rodrigue, L.P. Dunleavy, and P. Kirby, "Best practice for on-wafer millimeter wave noise figure measurements." *57th ARFTG Conference Digest*, Phoenix, AZ, 2001.

56. H. Meschede, R. Reuter, J. Albers, J. Kraus, D. Peters, W. Brockerhoff, F.-J. Tegude, M. Bode, J. Schubert, and W. Zander, "On-wafer microwave measurement setup for investigations on HEMTs and high-T_c superconductors at cryogenic temperatures down to 20 K." *IEEE Transactions on Microwave Theory and Techniques*, Vol. 40, No. 12, pp. 2325–2331, 1992.

57. J. Laskar, M.R. Murti, S.Y. Yoo, E. Gebara, and H.M. Harris, "Development of complete on-wafer cryogenic characterization: S-parameters, noise-parameters and load-pull." *1998 European GaAs and Related III–V Compounds, Application Symposium Digest*, Amsterdam, Netherlands, 1998. Pp. 33–38.

58. A. Caddemi, N. Donato, and M. Sannino, "Characterization techniques for temperature-dependent analysis of microwave transistors." *Proceedings of the 18th IEEE Instrumentation and Measurement Technology Conference 2001,* Vol. 3, 2001, Pp. 1893–1896.

59. J. Tuovinen, J. Varis, M. Lahdes, T. Karttaavi, and H. Hakojärvi, "Methods for on-wafer testing of cryogenic integrated circuits at millimetre waves." *Proceedings of the Fourth European Workshop on Low Temperature Electronics (WOLTE 4)*, Noordwijk, Netherlands, 2000. Pp. 157–162.

60. H. Rothe and W. Dahlke, "Theory of noisy four poles." *Proceedings of IRE*, Vol. 44, pp. 687–691, 1956.

61. "IRE standards on methods of measuring noise in linear twoports, 1959." *Proceedings of IRE*, Vol. 48, pp. 60–68, 1960.

62. R.Q. Lane, "The determination of device noise parameters." *Proceedings of the IEEE*, Vol. 57, No. 8, pp. 1461–1462, 1962.

63. M. Mitama and H. Katoh, "An improved computational method for noise parameter measurement." *IEEE Transactions on Microwave Theory and Techniques*, Vol. 27, No. 6, pp. 612–615, 1979.

64. G.I. Vasilescu, G. Alquie, and M. Krim, "Exact computation of two-port noise parameters." *Electronic Letters*, Vol. 25, No. 4, pp. 292–293, 1989.

65. A. Boudiaf, M. Laporte, J. Dangla, and G. Vernet, "Accuracy improvements in two-port noise parameter extraction method." *1992 IEEE MTT-S International Microwave Symposium Digest*, Albuquerque, NM, 1992, pp. 1569–1572.

66. L. Escotte, R. Plana, and J. Graffeuil, "Evaluation of noise parameter extraction methods." *IEEE Transactions on Microwave Theory and Techniques*, Vol. 41, No. 3, pp. 382–387, 1993.

67. M.W. Pospiezalski, "Modeling of noise parameters of MESFET's and MODFET's and their frequency and temperature depence." *IEEE Transactions on Microwave Theory and Techniques*, Vol. 37, No. 9, pp. 1340–1350, 1989.

68. P.J. Tasker, W. Reinert, J. Braunstein, and M. Schlechtweg, "Direct extraction of all four transistor noise parameters from a single noise figure measurement." *Proceedings of the 22nd European Microwave Conference*, Helsinki, Finland, 1992. Pp. 157–162.

69. A. Lazaro, L. Pradell, A. Beltran, and J.M. O'Callaghan, "Direct extraction of all four transistor noise parameters from 50 Ω noise figure measurements." *Electronics Letters*, Vol. 34, No. 3, pp. 289–291, 1998.

70. T. Karttaavi, *Transistor Modeling for a Millimeter Wave Low-Noise Amplifier*, Licentiate thesis, TKK Helsinki University of Technology, 2000.

71. V. Adamian and A. Uhlir, "A novel procedure for receiver noise characterisation." *IEEE Transactions on Instrumentation and Measurements*, Vol. 22, No. 6, pp. 181–182, 1973.

72. C.A. Davidson, B.W. Leake, and E. Strid, "Accuracy improvements in microwave noise parameter measurements." *IEEE Transactions on Microwave Theory and Techniques*, Vol. 37, No. 12, pp. 1973–1977, 1989.

73. R. Meierer and C. Tsironis, "An on-wafer noise parameter measurement technique with automatic receiver calibration." *Microwave Journal*, Vol. 38, No. 3, pp. 80–88, 1995.

74. A. Davidson, K. Jones, and E. Strid, "LRM and LRRM calibrations with automatic determination of load inductance", *36th ARFTG Conference Digest,* Monterey, 1990. Pp. 57–62.

75. Y.-L. Kok, M. DuFault, T.-W. Huang, and H. Wang, "A calibration procedure for W-band on-wafer testing." *1997 IEEE MTT-S International Microwave Symposium Digest*, Denver, CO, Vol. 3, 1997. Pp. 1663–1666.

76. R.B. Mark, "A multi-line method of network analyzer calibration." *IEEE Transactions on Microwave Theory and Techniques*, Vol. 39, No. 7, pp. 1205–1215, 1991.

77. R.T. Webster, A.J. Slobodnik Jr., and G.A. Roberts, "Determination of InP HEMT noise parameters and S-parameters to 60 GHz." *IEEE Transactions on Microwave Theory and Techniques*, Vol. 43, No. 6, pp. 1216–1225, 1995.

78. M. Lahdes, M. Sipilä, and J. Tuovinen, "60 GHz noise parameter measurements using cold-source method." *49th ARFTG Conference Digest*, Denver, 1997. Pp. 146–154.

79. M. Lahdes and J. Tuovinen, "V-band on-wafer noise parameter measurements." *Proceedings of GaAs 1998, The European Gallium Arsenide & Related III–V Compounds Applications Symposium*, Amsterdam, 1998. Pp. 39–44.

80. M. Lahdes, "Uncertainty analysis of V-band on-wafer noise parameter measurement system." *Proceedings of the 28th European Microwave Conference*, Amsterdam, Netherlands, 1998. Pp. 445–450.

81. T.A. Alam, R.D. Pollard, and C.M. Snowden, "The determination of on-wafer noise parameters at W-band." *Proceedings of the 27th European Microwave Conference*, Jerusalem, 1997. Pp. 687–691.

82. T.A. Alam, R.D. Pollard, and C.M. Snowden, "Determination of W-band noise parameters." *Electronic Letters*, Vol. 34, No. 3, pp. 288–289, 1998.

83. R. Drury, R.D. Pollard, and C.M. Snowden, "A 75–110 GHz automated tuner with exceptional range and repeatability." *IEEE Microwave Guided Wave Letters,* Vol. 6, No. 10, pp. 378–379, 1996.

84. R.E. Collin, *Foundations For Microwave Engineering*, New York, McGraw–Hill Book Company, 1966.

85. R. Ludvig, and P. Bretchko, *RF Circuit Design Theory and Applications*, Upper Saddle River, Prentice Hall, 2000.

86. D.M. Pozar, *Microwave Engineering*, New York, John Wiley & Sons, 1998.

87. G.M. Rebeiz, *RF MEMS: Theory, Design, and Technology*, New York, John Wiley & Sons, 2003.

88. G.E. Ponchak and L.P.B. Katehi, "Open- and short-circuit terminated series stubs in finite-width coplanar waveguide on silicon." *IEEE Transactions on Microwave Theory and Techniques*, Vol. 45, No. 6, pp. 970–976, 1997.

89. K. Hettak, N. Dib, A. Omar, G.Y. Delisle, M. Stubbs, and S. Toutain, "A useful new class of miniature CPW shunt stubs and its impact on millimeter-wave integrated circuits." *IEEE Transactions on Microwave Theory and Techniques*, Vol. 47, No. 12, pp. 2340–2349, 1999.

90. K. Hettak, C.J. Verver, and M.G. Stubbs, "Overlapping, multiple CPW stub structures for high density MMICs." *2001 IEEE MTT-S International Microwave Symposium Digest*, Phoenix, AZ, Vol. 1, 2001. Pp. 311–314.

91. V.S. Möttönen, J. Mallat, and A.V. Räisänen, "Characterisation of European millimetre wave planar diodes." *Proceedings of the 34th European Microwave Conference*, Amsterdam, Netherlands, 2004. Pp. 921–924.

92. L.E. Larson, R.H. Hackett, M.A Melendes, and R.F. Lohr, "Micromachined microwave actuator (MIMAC) technology – a new tuning approach for microwave integrated circuits." *Microwave and Millimeter-Wave Monolithic Circuits Symposium Digest*, Boston, MA, 1991. Pp. 27–30.

93. C. Goldsmith, J. Randall, S. Eshelman, T.H. Lin, D. Dennistor, S. Chen, and B. Norvell, "Characteristics of micromachined switches at microwave frequencies." *1996 IEEE MTT-S International Microwave Symposium Digest*, San Francisco, CA, 1996. Pp. 1141–1144.

94. C. Goldsmith, S. Eshelman, and D. Denniston, "Performance of low-loss RF MEMS capacitive switches." *IEEE Microwave and Guided Wave Letters*, Vol. 8, No. 8, pp. 269–271, 1998.

95. J.Y. Park, G.H. Kim, K.W. Chung, and J.U. Bong, "Fully integrated micromachined capacitive switches for RF applications." *2000 IEEE MTT-S International Microwave Symposium Digest*, Boston, MA, 2000. Pp. 283–286.

96. J.B. Muldavin and G.M. Rebeiz, "High isolation MEMS shunt switches; Part 1: Modeling." *IEEE Transactions on Microwave Theory and Techniques*, Vol. 48, No. 6, pp. 1045–1052, 2000.

97. J.B. Muldavin and G.M. Rebeiz, "High isolation MEMS shunt switches; Part 2: Design." *IEEE Transactions on Microwave Theory and Techniques*, Vol. 48, No. 6, pp. 1053–1056, 2000.

98. H.A.C. Tilmans, H. Ziad, H. Jansen, O. Di Monaco, A. Jourdain, W. De Raedth, X. Rottenburg, E. De Backerand, A. Decaussemaeker, and K. Baert, "Wafer-level packaged RF-MEMS switches fabricated in a CMOS fab." *Proceedings of International Electron Devices Meeting*, Washington DC, 2001. Pp. 41.4.1–41.4.4.

99. A. Abbaspour-Tamijani, L. Dussopt, and G.M. Rebeiz, "Miniature and tunable filters using MEMS capacitors." *IEEE Transactions on Microwave Theory and Techniques*, Vol. 51, No. 7, pp. 1878–1885, 2003.

100. J.S. Hayden, A. Malczewski, J. Kleber, C.L. Goldsmith, and G.M. Rebeiz, "2 and 4-bit DC-18 GHz microstrip MEMS distributed phase shifters." *2001 IEEE MTT-S International Microwave Symposium Digest*, Phoenix, AZ, 2001. Pp. 219–222.

101. J.S. Hayden and G.M. Rebeiz, "A low-loss Ka-band distributed MEMS 2-bit phase shifters using metal-air-metal capacitors." *2002 IEEE MTT-S International Microwave Symposium Digest*, Seattle, WA, 2002. Pp. 337–340.

102. J.S. Hayden and G.M. Rebeiz, "2-bit MEMS distributed X-band phase shifters." *IEEE Microwave and Guided Wave Lett*ers, Vol. 10, No. 12, pp. 540–542, 2000.

103. J.B. Rizk, *W-band RF MEMS Switches, Phase Shifters and Antennas*, Ph.D. dissertation, Department of Electrical Engineering, University of Michigan, Ann Arbor, MI, 2003.

104. J.S. Hayden, *High-Performance Digital X-Band and Ka-Band Distributed MEMS Phase Shifters*, Ph.D. dissertation, Department of Electrical Engineering, University of Michigan, Ann Arbor, MI, 2002.

105. V.M. Lubecke, W.R. McGrath, P.A. Stimson, and D.B. Rutledge, "Micromechanical tuning elements in a 620 GHz integrated circuit." *IEEE Transactions on Microwave Theory and Techniques,* Vol. 46, No. 8, pp. 2098–2103, 1998.

106. V.M. Lubecke, K. Mizuno, and G.M. Rebeiz, "Micromachining for Teraherz applications." *IEEE Transactions on Microwave Theory and Techniques,* Vol. 46, No. 11, pp. 1821–1831, 1998.

107. J.-C. Chiao, Y. Fu, I. Chio, M. DeLisio, and L.-Y. Lin, "MEMS reconfigurable Vee antenna." *1999 IEEE MTT-S International Microwave Symposium Digest*, Anaheim, CA, 1999. Pp. 1515–1518.

108. J.-C. Chiao, S.-Y. Cheng, J.J.L. Chang, I.M. Chio, Y. Kang, and J. Hayasaka, "MEMS reconfigurable antennas." *International Journal of RF and Microwave Computer Aided Eng*ineering, Vol. 11, No. 5, pp. 301–309, 2001.

109. W. Bischof, "Variable impedance tuner for MMIC's." *IEEE Microwave and Guided Wave Letters*, Vol. 4, No. 6, pp. 172–174, 1994.

110. C.E. McIntosh, R.D. Pollard, and R.E. Miles, "Novel MMIC source-impedance tuners for on-wafer microwave noise-parameter measurements." *IEEE Transactions on Microwave Theory and Techniques*, Vol. 47, No. 2, pp. 125–131, 1999.

111. J. de Mingo, A. Valdovinos, A. Crespo, D. Navarro, and P. García, "An RF electronically controlled impedance tuning network design and its application to an antenna input impedance automatic matching system." *IEEE Transactions on Microwave Theory and Techniques*, Vol. 52, No. 2, pp. 489–497, 2004.

112. H.-T. Kim, S. Jung, K. Kang, J.-H. Park, Y.-K. Kim, and Y. Kwon, "Low-Loss analog and digital micromachined impedance tuners at the Ka-band." *IEEE Transactions on Microwave Theory and Techniques*, Vol. 49, pp. 2394–2400, 2001.

113. J. Papapolymerou, K.L. Lange, C.L. Goldsmith, A. Malczewski, and J. Kleber, "Reconfigurable double-stub tuners using MEMS switches for intelligent RF front-ends." *IEEE Transactions on Microwave Theory and Techniques*, Vol. 51, No.1, pp. 271–278, 2003.

114. Y. Lu, D. Peroulis, S. Mohammadi, and L.P.B. Katehi, "A MEMS reconfigurable matching network for a class AB amplifier." *IEEE Microwave Wireless Components Letters*, Vol. 13, No. 10, pp. 437–439, 2003.

115. D. Qiao, R. Molfino, S.M. Lardizabal, B. Pillans, P.M. Asbeck, and G. Jerinic, "An intelligently controlled RF power amplifier with a reconfigurable MEMS-varactor tuner." *IEEE Transactions on Microwave Theory and Techniques*, Vol. 53, No. 3, pp. 1089–1095, 2005.

116. H. Nieminen, V. Ermolov, K. Nybergh, S. Silanto, and T. Ryhänen, "Microelectromechanical capacitors for RF applications." *Journal of Micromechanics and Microengineering*, Vol. 12, No. 2, pp. 177–186, 2002.

117. H. Nieminen, V. Ermolov, S. Silanto, K. Nybergh, and T. Ryhänen, "Design of a temperature-stable RF MEM capacitor." *IEEE Journal of Microelectromechanical Systems*, Vol. 13, No. 5, pp. 705–714, 2004.

118. H. Nieminen, J. Kankaanpää, V. Ermolov, S. Silanto, and T. Ryhänen, "RF MEMS for 0.8–2.5 GHz applications in mobile terminals." *MEMSWAVE 5th Workshop on MEMS for Millimeter Wave Communications*, Uppsala, Sweden, 2004. Pp. A42–A48.

119. K. Entesari and G.M. Rebeiz, "A 12–18 GHz three-pole RF MEMS tunable filter." *IEEE Transactions on Microwave Theory and Techniques*, Vol. 53, No. 8, pp. 2566–2571, 2005.

120. Q. Shen and N.S. Barker, "A reconfigurable RF MEMS double slug impedance tuner." *Proceedings of the 35th European Microwave Conference,* Paris, France, 2005. Pp. 537–540.

Appendix A: Detailed surface MEMS fabrication procedure used in this thesis

The fabrication process used in this thesis work is a modified six masks version from the surface MEMS process developed at the University of Michigan [103, 104]. Corning 7040 glass wafers with $\varepsilon_r = 4.6$ are used as substrates in this work, but the fabrication process is also suitable for other substrates. Only the exposing time of the photoresist in lithography should be adjusted according to the substrate material.

Fabrication steps

Resistive bias lines

1) Clean wafer with acetone and IPA. Blow dry with N_2.
2) Softbake at 80 ºC for 2 min. to remove all humidity.
3) Spin negative photoresist 5214 at 2000 rpm for 30 sec. Soft-bake at 105 ºC for 2 min. Align and expose 1.7 sec for quartz or glass wafers, 4.5 sec for silicon. Use Mask1. Hard-bake at 130 ºC for 90 sec. Flood expose 45 sec. Develop in AZ327 developer for 80 sec. Rinse in cascade DI water 2 min + 2 min. Blow dry with N_2. Use the microstripper (O_2 plasma) at 80 W and 250 mT for 2 min.
4) Sputter SiCr, 1200 Å. Parameters used in RF sputtering: Target number 2. 7 mT, 700 W, 18 min. Gas: Ar and N_2 (10 %).
5) Lift off in hot PRS1000 or PRS2000. Overnight soak is preferred. Rinse in DI water at least 15 min. Clean with acetone and IPA. Blow dry with N_2. Use the microstripper (O_2 plasma) at 150 W and 250 mT for 3 min to remove photoresist and other organic scums.

First metal layer

1) Softbake at 80 ºC for 2 min. to remove all humidity.

2) Spin negative photoresist 5214 at 2000 rpm for 30 sec. Soft-bake at 105 ºC for 2 min. Align and expose 1.7 sec for quartz or glass wafers, 4.5 sec for silicon. Use Mask1. Hard-bake at 130 ºC for 90 sec. Flood expose 45 sec. Develop in AZ327 developer for 80 sec. Rinse in cascade DI water 2 min + 2 min. Blow dry with N_2. Use the microstripper (O_2 plasma) at 80 W and 250 mT for 2 min.

3) Blow the wafer with N_2 just before putting it to the evaporator. Evaporate Ti/Au/Ti, 500 Å/5000 Å/500 Å.

4) Lift off in hot PRS1000 or PRS2000. Overnight soak is preferred. Rinse in DI water at least 15 min. Clean with acetone and IPA. Blow dry with N_2. Use the microstripper (O_2 plasma) at 150 W and 250 mT for 3 min to remove photoresist and other organic scums.

Silicon nitride dielectric layer

1) Deposit Si_3N_4, 2000 Å, with the PECVD. Use the following paramters: SiH_4 = 100 sccm, NH_3 = 10 sccm, He = 900 sccm, N_2 = 990 sccm, pressure = 700 mT, power = 100 W, temperature = 400 ºC, time = 12 min.

2) Softbake at 80 ºC for 2 min. Spin HMDS adhesion promoter at 3000 rpm for 30 sec. Spin photoresist 1813 or 1827 at 3000 rpm for 30 sec. Soft-bake at 105 ºC for 2 min. Align and expose 7 sec for 1813 and 15 sec for 1827. Use Mask3. Develop in diluted MF 351 developer for 45 sec. Rinse in cascade DI water 2 min + 2 min. Blow dry with N_2. Hard-bake at 130 ºC for 2 min. Clean the wafer with the microstripper (O_2 plasma) at 150 W and 250 mT for 2 min.

3) Pattern the Si_3N_4 with RIE using next parameters: CF4 = 40 sccm, O2 = 1 sccm, pressure = 100 mT, power = 100 W, time = 12 min (includes some over etching).

4) Flood expose 90 sec. Develop in diluted MF351 90 sec. Rinse in cascade DI water 1 min + 1 min. Blow dry with N_2. Strip the remaining

photoresist in hot PRS1000 or PRS2000 at least 3 hours. Rinse in DI water at least 15 min. Clean with acetone and IPA. Blow dry with N_2. Clean with the microstripper (O_2 plasma) at 150 W and 250 mT for 3 min.

Sacrificial layer

1) Softbake at 80 ºC for 2 min. Spin HMDS at 3000 rpm for 30 sec.
2) Spin PMMA 950K 9 % at 2300 RPM for 45 sec. to get about 1.3–1.5 um.
3) Bake in an oven at 170 ºC for 30 min.
4) Evaporate or sputter Ti, 2000 Å, to be used as a mask for the PMMA patterning.
5) Soft-bake at 80 ºC for 2 min. Spin HMDS at 3000 rpm for 30 sec. Spin positive photoresist 1827 at 3000 rpm for 30 sec. Softbake at 105 ºC for 30 sec. Align and expose 15 sec with Mask4. Develop in diluted MF351 45 sec. Rinse in cascade DI water 2 min + 2 min. Blow dry with N_2. Softbake at 80 ºC for 30 sec, softbake at 105 ºC for 30 sec, hardbake at 130 ºC for 90 sec.
6) Etch Ti with HF:DI (1:20). Ti etch takes just a few seconds. Watch for bubble coming out. Rinse in DI water for 3 min. Blow dry with N_2.
7) Flood expose 90 sec and develop in diluted MF351 2 min. Rinse in cascade DI water 2 min + 2 min. Blow dry with N_2. Do not clean with the microstripper (O_2 plasma) because it etches the PMMA sacrificial layer.
8) Etch PMMA in RIE. Recipe 1: O_2 = 100 sccm, pressure = 50 mT, power = 250 W, time = 21 min (etch 90 sec, RF off 60 sec). An other possibility is to use O_2 = 20 sccm, pressure = 20 mT, power = 50 W, time = 30 min (this is continuous etch).
9) Etch the Ti mask with HF:DI (1:20). Rinse in DI water for 3 min. Blow dry with N_2.

Structural layer deposition

Sputter Ti/Au/Ti, 100 Å/8000 Å/100 Å. Sputtering parameters: Ti: 7 mT, target 1, 650 W, deposition rate 50 Å/min (20 rpm). Au: 10 mT, target 3, 0.5 A, time = 30 min, (20 rpm).

Gold electroplating

1) Soft-bake at 80 ºC for 2 min. Spin HMDS at 3000 rpm for 30 sec. Spin positive photoresist 1827 at 3000 rpm for 30 sec. Softbake at 105 ºC for 30 sec. Align and expose 15 sec with Mask5. Develop in diluted MF351 45 sec. Rinse in cascade DI water 2 min + 2 min. Blow dry with N_2. Softbake at 105 ºC for 2 min to improve photoresist adhesion.
2) Etch Ti with HF:DI (1:20). Rinse in DI water for 3 min. Blow dry with N_2. Softbake at 105 ºC for 1 min.
3) Electroplate 3–5 μm of Au. Parameters for the gold plating: Plating solution either Arotemp 24 ($Ka(CN)_2$) and DI water or BDT 510. Temperature of the solution = 50–55 ºC. Current density = 10 mA, stirrer speed = 200 rpm (increases plating uniformity). Rinse in DI water 2 min and blow with N_2.
4) Flood expose 90 sec. Develop in diluted MF351 2 min. Rinse in cascade DI water 2 min + 2 min. Blow dry with N_2.

Structural layer annealing

1) Softbake at 80 ºC for 2 min on a hot plate.
2) Softbake at 105 ºC for 2 min on a hot plate.
3) Hardbake at 130 ºC for 2 min on a hot plate.
4) Hardbake at 150 ºC for 2 min on a hot plate.
5) Bake in an oven at 170 ºC for 3 min.

The wafer needs to be transferred quickly between the hot plates.

Other possibility is to use just one hot plate and temperature ramp from 80 ºC to 150 ºC totally 8 min and then to the oven for 3 min and 170 ºC.

Structural layer patterning and release

1) Softbake at 80 ºC for 2 min. Spin HMDS at 3000 rpm for 30 sec. Spin positive photoresist 1827 at 3000 rpm for 30 sec. Softbake at 105 ºC for 1 min. Align and expose 15 sec with Mask6. Develop in diluted MF351 45 sec. Rinse in cascade DI water 2 min + 2 min. Blow dry with N_2. Softbake at 105 ºC for 2 min to improve photoresist adhesion.
2) Etch Ti with HF:DI (1:20). Rinse in DI water for 3 min. Blow dry with N_2.
3) Etch Au with TFA gold etchant. Rinse in DI water for 3 min. Blow dry with N_2.
4) Flood expose 90 sec and d evelop in diluted MF351 90 sec. Rinse in cascade DI water 2 min + 2 min. Blow dry with N_2.
5) Etch remaining Ti with HF:DI (1:20). Rinse in DI water for 3 min. Blow dry with N_2.
6) Remove sacrificial layer by soaking in PRS2000 at least 3 hours, preferably overnight.
7) Rinse in DI water 15 min, without bubbles. Do not blow dry.
8) Soak in acetone 3 hours. This is optional but ensures that all PMMA and PRS2000 is removed.
9) Soak in IPA 15 min + 15 min.
10) Transfer to ethanol.
11) Transfer to the critical point dryer. Try the wafer in the critical point dryer.

Published by	Series title, number and report code of publication
VTT	VTT Publications 596 VTT–PUBS–596

Author(s)

Vähä-Heikkilä, Tauno

Title

MEMS tuning and matching circuits, and millimeter wave on-wafer measurements

Abstract

The focus of this thesis is on the development of on-wafer measurement techniques for millimeter wave device and circuit characterization as well as on the development of MEMS based impedance tuning circuits both for measurement and telecommunication applications. Work done in this thesis is presented with eight scientific articles written by the author. The summary of the thesis introduces the field of on-wafer measurements and impedance tuning methods, and is followed by the articles.

Wide-band on-wafer measurement systems have been developed for noise parameter measurement at room temperature at W-band, and for cryogenic S-parameter measurements at 50–110 GHz and 20–295 K. Using the developed systems, noise parameters of an InP HEMT have been measured and results are shown in the frequency band of 79–94 GHz. These are the first published noise parameter measurement results for an active device at W-band, and first on-wafer measurement results at cryogenic conditions and at 50–110 GHz.

Novel RF MEMS impedance tuners have been developed for instrumentation and measurement applications to improve measurement automation and accuracy in on-wafer measurements. Several integrated impedance tuners have been realized to cover 6–120 GHz frequency range. RF MEMS technology has also been used for reconfigurable matching networks. Reconfigurable distributed 4–18 GHz and 30–50 GHz matching networks have been designed, fabricated, and characterized. These are based on switched 4 or 8 MEMS capacitors producing 16 or 256 different impedances. The matching networks are ideal for multi-band and wide impedance range amplifier as well as for antenna matching and tuning applications. Both the tuners and matching networks have shown state-of-the-art performance for circuits realized with integrated circuit technologies.

Keywords

RF MEMS, on-wafer measuring techniques, millimeter wave devices, impedance tuning, instrumentation, noise parameter measurements, reconfigurable matching networks, W-band measurement, double-stub tuners, triple-stub tuners, amplifier applications

ISBN

951–38–6704–8 (nid.)

951–38–6705–6 (URL: http://www.vtt.fi/publications/index.jsp)

Series title and ISSN		Project number	
VTT Publications 1235–0621 (nid.) 1455–0849 (URL: http://www.vtt.fi/publications/index.jsp)			
Date March 2006	Language English, Finnish abstr.	Pages 86 p. + app. 82 p.	Price D
Name of project MEMSTUNER		Commissioned by	
Contact VTT Technical Research Centre of Finland Tietotie 3, P.O. Box 1000, FI-02044 VTT, Finland Phone internat. +358 20 722 111 Fax +358 20 722 7012		Sold by VTT Technical Research Centre of Finland PL 1000, 02044 VTT Puh. 020 722 4404 Faksi 020 722 4374	

Julkaisija

VTT

Julkaisun sarja, numero ja raporttikoodi

VTT Publications 596
VTT–PUBS–596

Tekijä(t)
Vähä-Heikkilä, Tauno

Nimeke

Mikromekaaniset viritys- ja sovituspiirit sekä millimetri-aaltoalueen suoraan kiekolta tehtävät mittaukset

Tiivistelmä

Väitöskirjatyössä kehitettiin suoraan kiekolta tehtäviä millimetriaaltoalueen mittauksia sekä mikromekaanisia (MEMS) impedanssin säätö- ja sovituspiirejä.

Mittauslaitteistoja ja -menetelmiä kehitettiin suoraan kiekolta tehtäviin mittauksiin millimetriaaltoalueelle. Kohinaparametrien mittaamiseksi kehitettiin laitteisto W-alueelle (75–110 GHz), ja mittaustulokset esitetään InP HEMT -transistorille 79–94 GHz taajuusalueella. Sirontaparametrien mittaamiseksi kryogeenisissä olosuhteissa kehitettiin laitteisto W-alueelle, ja laajakaistaiset sekä kahden aaltoputkikaistan kattavat mittaustulokset esitetään InP HEMT -transistoreille 50–110 GHz:n taajuusalueella ja 20–295 K:n lämpötiloissa. Sekä molemmat mittauslaitteistot että esitettävät tulokset ovat ainutlaatuisia näillä taajuuksilla.

Kohinaparametrimittauslaitteistojen kehittämiseksi ja mittausten automatisoimiseksi väitöskirjatyössä suunniteltiin ja valmistettiin integroituja mikromekaanisia impedanssivirittimiä. Impedanssivirittimillä tuotetaan erilaisia impedansseja, ja niitä voidaan kontrolloida sähköisesti. Impedanssin säätö perustuu MEMS-kondensaattoreihin, ja kehitetyillä piireillä saadaan tuotettua tuhansia erilaisia impedansseja riippuen MEMS-kondensaattoreiden lukumäärästä. Impedanssivirittimiä kehitettiin usealle eri taajuusalueelle taajuuksien 6 ja 120 GHz välille. Virittimien tuottama heijastuskerroin on parhaimmillaan lähellä yhtä mitatun seisovan aallon suhteen ollessa 199 taajuudella 30 GHz. Työssä myös sovellettiin MEMS-kondensaattoreita impedanssinsovituspiireihin tehovahvistimen ja antennin sovittamiseksi. Piireissä integroidun siirtolinjan sähköistä pituutta ja impedanssia muutetaan. Mitatut tulokset osoittavat, että piireillä voidaan sovittaa paljon erilaisia impedansseja pienin häviöin ja lineaarisesti.

Avainsanat
RF MEMS, on-wafer measuring techniques, millimeter wave devices, impedance tuning, instrumentation, noise parameter measurements, reconfigurable matching networks, W-band measurement, double-stub tuners, triple-stub tuners, amplifier applications

ISBN
951–38–6704–8 (nid.)
951–38–6705–6 (URL: http://www.vtt.fi/publications/index.jsp)

Avainnimeke ja ISSN
VTT Publications
1235–0621 (nid.)
1455–0849 (URL: http://www.vtt.fi/publications/index.jsp)

Projektinumero

Julkaisuaika	Kieli	Sivuja	Hinta
Maaliskuu 2006	Englanti, suom. tiiv.	86 s. + liitt. 82 s.	D

Projektin nimi
MEMSTUNER

Toimeksiantaja(t)

Yhteystiedot
VTT
Tietotie 3, PL 1000, 02044 VTT
Puh. vaihde 020 722 111
Faksi 020 722 7012

Myynti
VTT
PL 1000, 02044 VTT
Puh. 020 722 4404
Faksi 020 722 4374

VTT PUBLICATIONS 596 MEMS tuning and matching circuits, and millimeter wave on-wafer measurements Tauno Vähä-Heikkilä

This work deals with millimeter wave on-wafer measurement techniques for device and circuit characterization as well as with MicroElectroMechnical Systems (MEMS) based impedance tuning and matching circuits both for measurement and telecommunication applications. This thesis work has produced new knowledge and scientific results in the following areas: 1) cryogenic on-wafer measurements at millimeter wavelengths; 2) on-wafer noise parameter measurement methods and a system for W-band device characterization; 3) novel impedance tuners for measurement applications based on RF MEMS technology; and 4) novel reconfigurable matching networks for telecommunication applications based on RF MEMS technology. The work includes on-wafer measurement system development, RF MEMS circuit design, fabrication, and characterization which are described in the thesis.

Tätä julkaisua myy	Denna publikation säljs av	This publication is available from
VTT	VTT	VTT
PL 1000	PB 1000	P.O. Box 1000
02044 VTT	02044 VTT	FI-02044 VTT, Finland
Puh. 020 722 4404	Tel. 020 722 4404	Phone internat. +358 20 722 4404
Faksi 020 722 4374	Fax 020 722 4374	Fax +358 20 722 4374

ISBN 951- 38- 6704- 8 (soft back ed.)
ISSN 1235- 0621 (soft back ed.)

ISBN 951- 38- 6705- 6 (URL: http://www.vtt.fi/inf/pdf/)
ISSN 1455- 0849 (URL: http://www.vtt.fi/inf/pdf/)